Phobos, Deimos: Formation and Evolution

Alex Soumbatov-Gur

Phobos, Deimos: Formation and Evolution

Alex Soumbatov-Gur

The moons are confirmed to be ejected parts of Mars' crust. After explosive throwing out as cone-like rocks they plastically evolved with density decays and materials transformations. Their expansion evolutions were accompanied by global ruptures and small scale rock ejections with concurrent crater formations. The scenario reconciles orbital and physical parameters of the moons. It coherently explains dozens of their properties including spectra, appearances, size differences, crater locations, fracture symmetries, orbits, evolution trends, geologic activity, Phobos' grooves, mechanism of their origin, etc. The ejective approach is also discussed in the context of observational data on near-Earth asteroids, main belt asteroids Steins, Vesta, and Mars. The approach incorporates known fission mechanism of formation of miniature asteroids, logically accounts for its outliers, and naturally explains formations of small celestial bodies of various sizes.

Contents

1 Introduction

The problem of origins of the natural Martian moons has been discussing by astrophysical community since the discovery of Phobos and Deimos in 1877 [1]. In spite of abundant observations the issue of their histories and compositions is still open. No scenario consistently explains the bulk of parameters of the Martian satellites. The reconciliation of their physical and dynamical characteristics is a stumbling block of majority of schemes being proposed.

There are two major groups of hypotheses about origins of the moons. The first is that the satellites are asteroids captured by Mars. Their surface reflective and spectral parameters are roughly similar to D-type asteroids (carbonaceous chondrites). The second hypothetical group considers accretion scenarios. They suppose formation of the moons due to accretion of primordial planetesimals simultaneously with Mars or their later accretion build-up from Martian ejecta thrown out by severe outer impact.

The capture scenario is very problematic dynamically because changing from parabolic to elliptical trajectory needs the loss of kinetic energy due to dissipation e.g. in the atmosphere of the red planet. But Mars' atmosphere is thin and is not adequate to slow down captured bodies. Besides, the orbits of both moons are strangely placed in equatorial plain of Mars. Accretion scenarios also meet difficulties. They are spectral and compositional ones. Short account of the theoretical problems with the emphasis on contemporary plans of space exploration of Mars and its moons is given in [2]. As it was pointed out in review [1] successful theory is to explain orbital dynamics, morphology, low densities, ages, geology, and evolution trends of the satellites.

This report proposes and evidences a new consistent approach to the origins and histories of the Martian satellites. It is based on our general expansion/ejection model of the formation of small celestial bodies that was applied to several main belt and near-Earth asteroids in [3,4,5]. The heart of the ejective rationale is that larger bodies give births to smaller ones. In the labor process a rock body is formed inside the mantle and/or crust of its parent body due to intrinsic crack development. Then an offspring is explosively ejected rotated out into the orbit of its primary to become a satellite. After formation of a body its evolution trend is plastic elongation or plastic expansion into spherical shape. Both evolution types are accompanied by ejections of smaller scales.

Further we give evidences that Phobos and Deimos were initially formed inside Martian crust and were explosively thrown into orbits around Mars. After their formations the Martian satellites expanded from initial cone-like shapes owing to slow plastic evolution with strong morphology changes and corresponding density decays. The evolution of the moons was interspersed by rock ejections, crater formations, and rupture developments.

In the following we shortly consider some features of our approach and explore evolution trends of several main belt and near-Earth asteroids to provide clues to further analyses of the Martian satellites. Then we explain parameters and features of Phobos and Deimos from the unifying point of view of expansive/ejective morphogenesis. In Discussion section we analyze related issues for Phobos, Deimos, and Mars as well as confer unifying scenario for originations of small celestial bodies.

2 Some properties of expansive/ejective morphogenesis

We consider all celestial bodies as open thermodynamic systems exchanging energy and matter with their ambient. Our integral approach states that small solid celestial bodies form in result of larger bodies' explosive fracture processes and retain some of their symmetries and properties [3,4,5]. After ejection both parent and offspring still undergone slow plastic evolvement punctuated by ejective events and shape modifications. Given some conditions are fulfilled morphology and composition changes happen including explosive ejections of rocks, boulders, and particles of different sizes. In case of rather slow and small exchange intensity the plastic reshaping of a rigid body also proceeds slowly and gradually. The smaller is a body, the quicker it evolves. The unified evolutional approach is equally applicable to asteroids, comets, and satellites. Its essential feature is scale invariance. That allows for analyses of similar geometries of small celestial bodies in spite of orders of magnitude differences in their dimensions and drastic spectral diversities.

An ejection is generally a solid state phenomenon. Expansion of a celestial body leads to the development of local mechanical stresses on its surface and inside. It is well known in solid state physics and fracture mechanics that in case of stress application all discontinuities and imperfections concentrate stresses in their vicinities. As a rule, in the area about the characteristic size of an imperfection they rise several times, compared to those far-off. Under some additional conditions stress concentrations may lead to partial or complete destruction of a solid body due to brittle or ductile fracture.

When a crack develops and elongates along body's surface or perpendicular to it an endogenous crater with simultaneous cone bulk rock and/or debris ejection may form. Mechanical energy of a stressed crack spends on formation its new surface in case of brittle fracture and plastic deformations near crack opening in case of more energy consuming plastic changes due to ductile fracture. The process is thermodynamically profitable for cracks longer than critical or stresses higher than critical. The size of an endogenous crater is as indicator of fracture depth.

The parameters of plastic deformation zone around crack opening depend upon crustal layer geometry and existing stresses. In mechanical modeling the limiting cases are plain stress and plain strain conditions inside crustal layer. Correspondingly the zone varies from rounded volume to bean and even dumbbell shaped one in cross-section. Therefore the appearance of rounded plastic zone inside forming cone or pyramid-shaped rock may give rise to the creation of inner nucleus and concentric material layers inside. Besides, a conical rock is usually layered parallel to its base plane due to the layered structure of parental crust. Bean and dumbbell shaped plastic zones may result in formation of twin craters with ejection of concomitant twin rock bodies. In those cases crack remnant line usually symmetrically divides double craters along their contact border.

For further analyses we notice that lined crater assemblies (catenae) as a rule are surface markings of faults and fractures underlying them. Sometimes both crack lines and concavities are noticeable on surfaces of celestial bodies. Occasionally crack lines are not seen at all. Occasionally in result of local substance modifications without ejections fractures are marked by regular elevations of different sizes.

3 Clues to the 00analyses of Phobos and Deimos

3.1 Asteroid (2867) Steins

We considered the appearance and features of main belt asteroid (2867) Steins in [4]. The asteroid was encountered by ESA's Rosetta spacecraft on 5 September 2008 [6,7]. It was shown that the asteroid of ideal brilliant cut shape (fig.1) was ejected rotated around its axis of symmetry (shortest axis Z) into space out of the crust of some larger parent body [4,5] .

Steins (6.83x5.70x4.42km) is at initial evolutionary stages of plastic elongation and growth. That is demonstrated e.g. by existence of large Northern crater Diamond and a catena, that divides the asteroid almost by half. The catena is seen in all views of fig.1 except the upper left one. Steins' cone apex is a bit elongated and is crossed by global fracture marked by the catena. The apex is separated i.e. the southern polar region has saddle morphology due to expansion along the largest (X) axis of the asteroid.

The asteroid equator contains approx. regular craters. The whole Steins' appearance proves stress symmetries in North-South, East-West directions and 45° to them. The reason is the interplay of primary tensions and shears which arise because of symmetrical shape and elongations in X direction. Steins bears special surface features which are connected to its plastic reshaping [4].

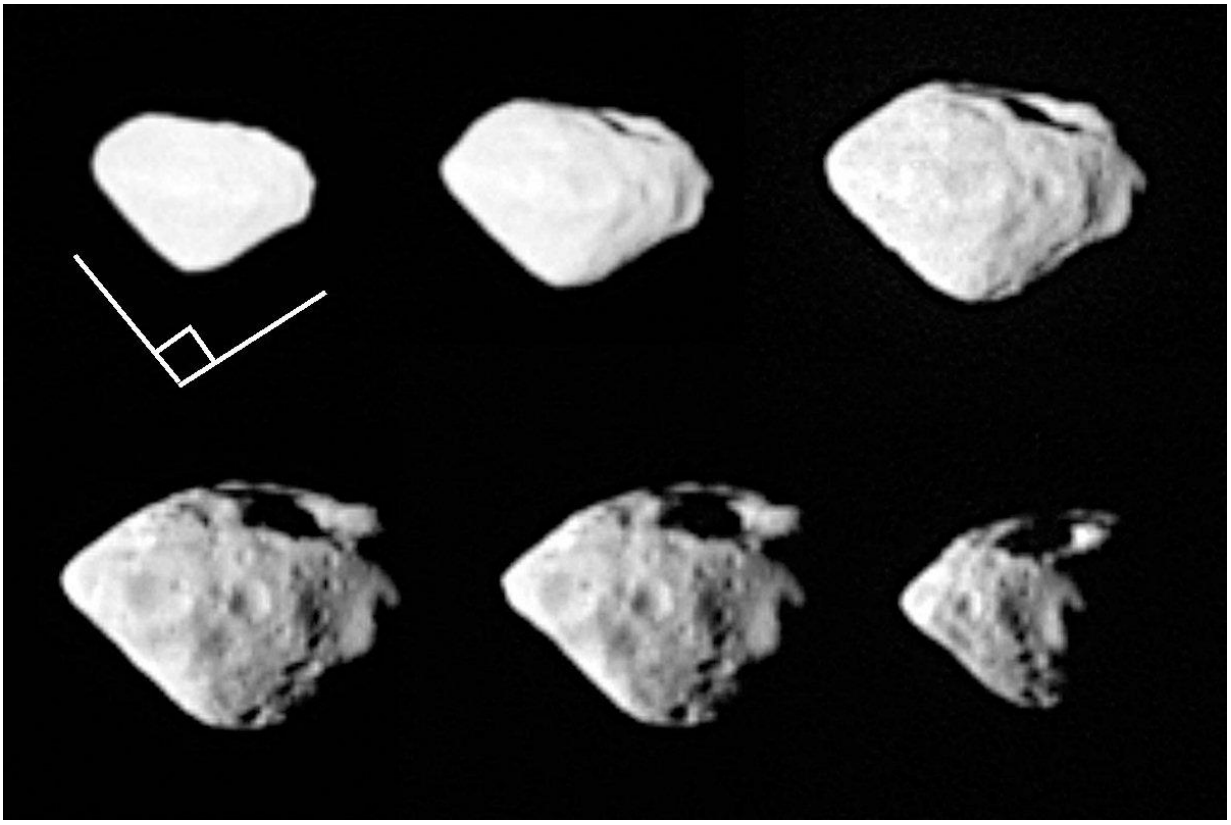

Fig.1. Six views of approx two thirds of Steins' surface acquired by OSIRIS imaging system before, during, and after the close encounter. White sketch was added by us to emphasize ca. 90° northern pole summit angle. (http://www.esa.int/spaceinimages/Images/2008/09/Asteroid_Steins_A_diamond_in_space)

Our analyses of Steins and other celestial bodies lead us to the conclusion that expansion/ejection morphogenesis is not homogenous over bodies' volumes but proceeds in special directions and in local regions. Therefore it is sometimes possible to find angles of view to largely ignore shape changes of a plastically evolving body (e.g. upper left view in fig 1). That greatly helps decipher initial shapes of small celestial objects. For example, Deimos resembles cone in some viewing directions (fig.2 left).

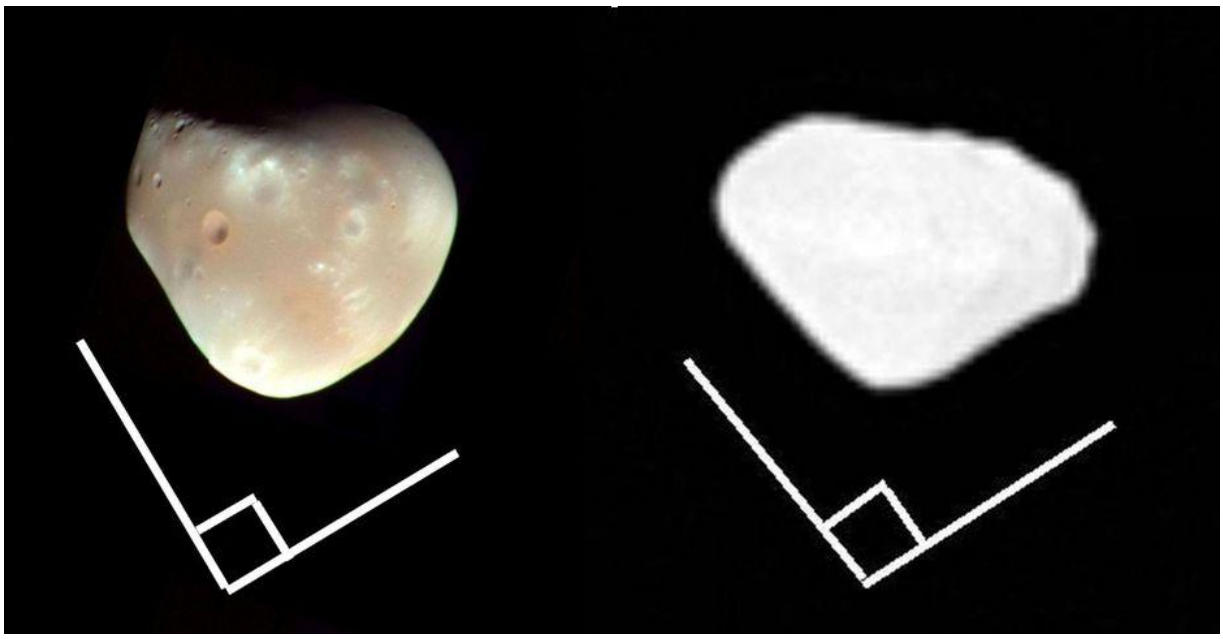

Fig.2. Comparison of Deimos' and Steins' geometries. White sketches emphasize summit angles close to 90°. The right view is the part of fig.1. The left view is rotated color enhanced image of Deimos, captured by the Mars Reconnaissance Orbiter on 21 February 2009.
(en.wikipedia.org/wiki/Deimos_(moon)#/media/File:Deimos-MRO.jpg)

Steins is also comparable to Deimos in general surface topography, particularly in slope statistics. Slopes are angles between the local surface normal and the local acceleration vector summing gravitational and centrifugal ones. The distribution of Steins' local slopes implying density about 1.8 g/cc was measured in [7]. It was found no clear enhancement at big slope angles. The large extent of the smooth terrain with shallow slopes less than 15° is also consistent with the observed lack of photometric variations of the single scattering albedo [8]. The resemblance of Steins and Deimos may be also related to thick regolith blanket covering their surfaces and evolution plastic reshaping of them.

3.2 Small near-Earth asteroids

We considered morphologies of some freshly ejected near-Earth asteroids in [5]. One of the objects studied was (66391)1999 KW4 binary asteroid with primary ca. 1.5km in size and density 2g/cc (fig.3). It is top-like (cone-like) in shapes and has a large concavity on its prominent equatorial ridge. The secondary of the size of that concavity is at spin-orbit lock. The satellite's longer X axis (see fig.4.) is directed to the primary [9,10].

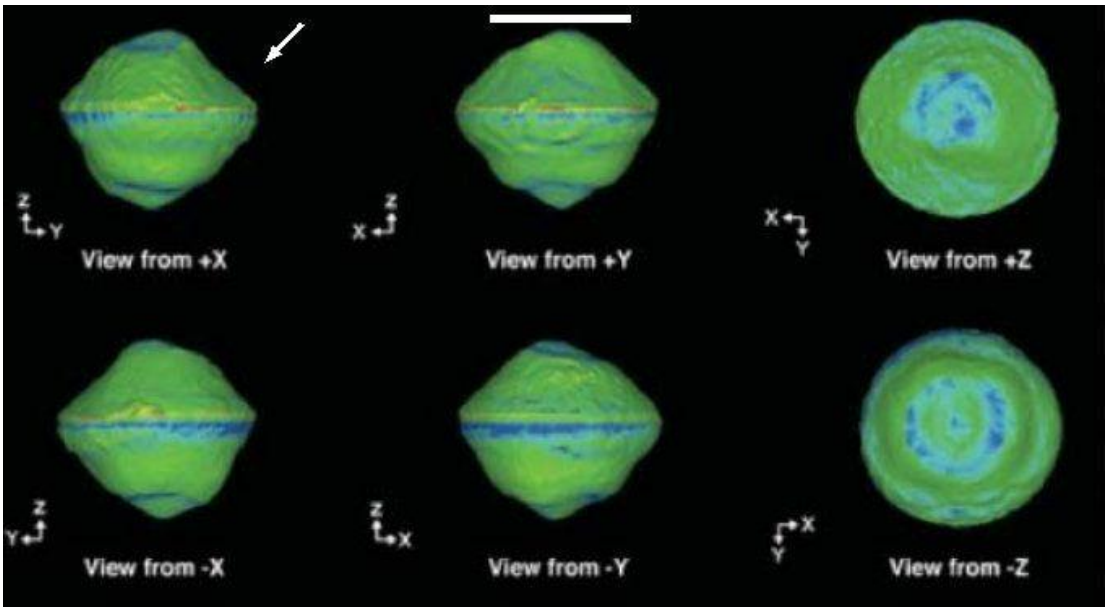

Fig.3. Axial views of KW4 primary asteroid [9]. Scale mark is 1km. Arrow points to a concavity located face-on in view from +Y. Colors from blue to red indicate calculated effective gravitational slope (0-75°).

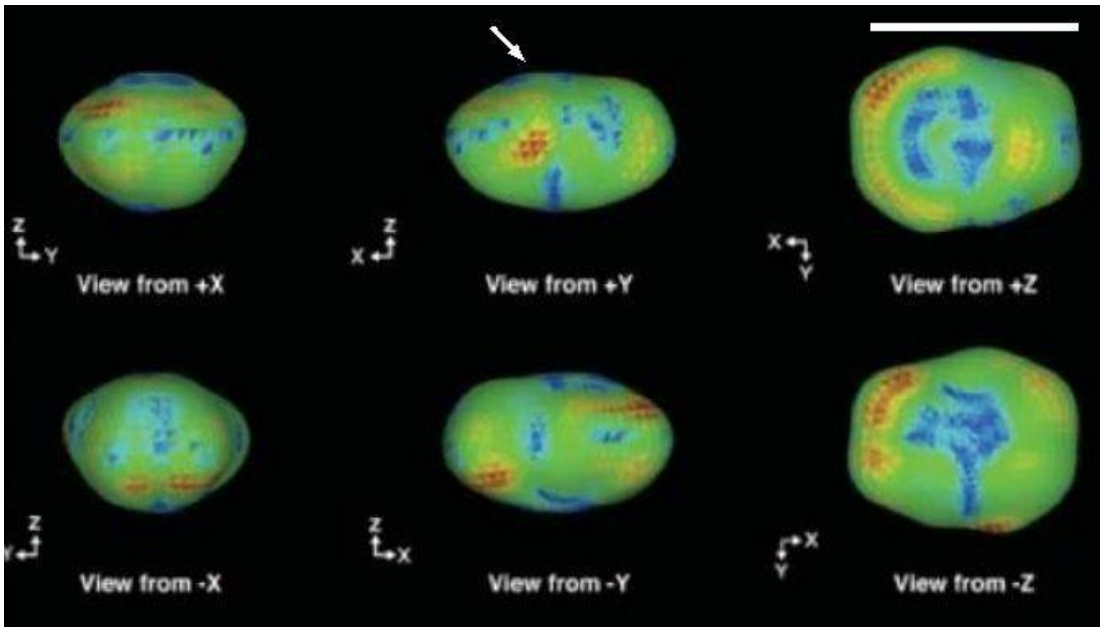

Fig.4. Axial views of KW4 satellite asteroid [9]. Scale mark is 500m. Arrow marks possible northern boulder. X axis points toward primary asteroid. Colors from blue to red indicate calculated local effective gravitational slope (0-20°). Notice that color lines are prone to be straight and parallel to the axes.

According to our rationale the secondary which is strangely tens percents denser than the primary was a coherent part of it earlier. Later the satellite was ejected with simultaneous concavity formation, the density anomaly being explained by the denser material composition [3,4] of the singular region the concavity was formed in.

The shape of the secondary is not faceted. It is round in contrast to the primary. The reason is that the plastic evolution of the smaller object is more rapid compared to the larger one. The whole shape impression is the expansion in all three directions, the one along X axis being the largest. Note that the X-axis views (fig.4, left column) still retain cone impression.

Colors of the figures reflect gravitational slopes i.e. angular deviations of the local downward normal from the local sum acceleration vector (due to gravity and rotation). The average primary's slope is 28° (max. 70°), whereas the secondary's - 9° (max. 18°). Several times smaller average and maximal slopes appear to result from plastic evolution of the satellite.

Color figures allow for the analysis of symmetries of the satellite parts. Polar views in fig.4 are shown in the right column. The region around the northern pole looks round and seems to contain large craters and boulders. The southern pole appears to be angular. The equatorial belt seems to contain regular concavities. There is size difference of +X and –X parts of the satellite, the latter being the smaller. The satellite appears to be divided by half along X and Y axes by fractures, the more color discernable one being directed along Y axis. The plausible reason of 90° fracture crossing is high symmetry of the primary and its concavity (see fig.3, view from +Y).

Another representative of cone-like objects with equatorial ridge, uniformly sloped sides, polar flattening, and elongated satellites is triple asteroid (136617) 1994 CC [11]. Due to high eccentricity 1994 CC crosses both Earth's and Mars' orbits. The primary asteroid is ca 0.7km wide, top-like, and slightly elongated. The inner and outer satellites are 112m and 80m in size, respectively. The larger has synchronous orbit with semi-major axis of 1.7km and negligible eccentricity (0.002). The outer satellite is not synchronous and has six times smaller mass. Its eccentric orbit (e=0.192) is inclined at 16° to that of the inner satellite. The orbit (s.m.a. equals 5.7km) is very large for multiple asteroids. The case of 1994 CC is common among multiple systems of near-Earth asteroids. Triples comprise one percent of the entire near-Earth population observed by radars. The other two clearly identified triple systems are (153591) 2001 SN263 and 3122 Florence.

It is said in [11] that "the discovery of triple systems in the NEA population generates even more questions than were raised initially with the discovery of binaries." For instance, if more than two satellites could exist? What is the origin and lifespan of satellites? To our opinion triple near-Earth satellites could be observational objects to verify the ideas put forward in this report. The amount of satellites and meaningful eccentricities suggest intensified energy exchanges with the ambient and inside triple systems. They are also suspicious for smaller satellite ejections by their larger satellites. Further discussion on the matter is given in section 5.4.

3.3 Asteroid (4) Vesta

As a rule, the more round is a celestial body, the less characteristic features of its childhood are left. Main belt asteroid (4) Vesta looks almost as dwarf planet (1) Ceres, but its profile proves that the asteroid saves some of its initial shape (fig.5). Vestan southern pole geometry is usually seen as enormous basins Veneneia and Rheasilvia formed in result of two brutal outer impacts, strangely into the same area, which Vesta amazingly survived [12]. Opposite, we think that Vesta's shape is the result of the plastic rounding of a cone-like object initially ejected by some larger celestial body.

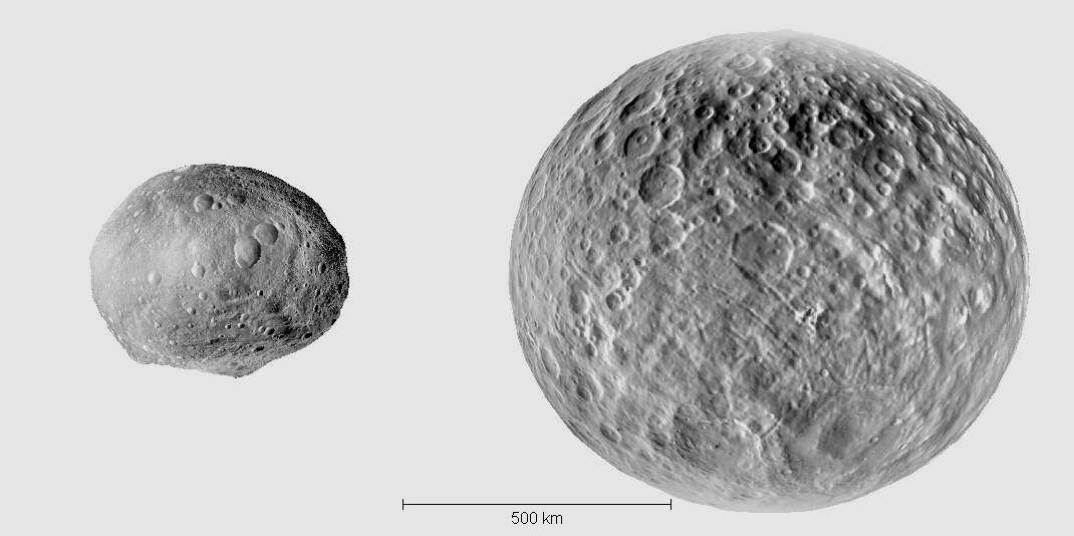

Fig.5. Views of asteroid Vesta (left) and dwarf planet Ceres (right). The original image was converted into black and white, scaled, inverted, and contrasted. (www.photojournal.jpl.nasa.gov./catalog/pia21081)

The main sizes of Vesta are a bit different, 286km (X), 279km (Y), and 223km (Z) [13,14]. The shortest Z axis of the asteroid is its rotational axis. Those differences and rotation direction are natural for explosively ejected conical bodies [4,5]. The cone apex remnant at the southern pole is about 20km high. Vesta is a stratified asteroid and is supposed to have mantle and hundred kilometers core. Vestan density 3.5g/cc belongs to the range of Martian crust [15, 16].

Multispectral images acquired by Dawn expose global color variations that uncover hemispherical dichotomy [17]. The same asymmetry is revealed in hydrogen contents [18] or in OH containing materials of the crust [19]. Cratering record of Vesta also has a strong dichotomy. It is said in [20] that Vesta's northern heavily cratered terrains retain much of craters' earliest history. Vesta's crust is supposed to form by melting [13]. It is broadly consistent with high temperature methamorphism [21].

North-south dichotomy of Vesta is the normal feature of ejective orogenesis. The base part of cone or pyramid-like offspring body is the remnant of parental surface. Contrary, cone part results from explosively shocked and highly modified underground materials. By the by, for Pluto's satellite Charon the ejective pyramid model immediately explains existence of Mordor Macula, its polar location, its composition, and its angular geometry, coincident to that of Sputnik Planitia.

The symmetry of primary tensions and shears, that is East-West, North-South, and 45° to them, is always reflected in morphology, fractures, and inner structure of ejected bodies. The same holds for Vesta. One may notice in figs.6,9 that rounded Vesta retains some of four-fold symmetries like above discussed satellite of asteroid 1999 KW4. The same symmetries are revealed in the asteroid topography and gravity (fig.7) as well as proved by 45° angle between the rotation axis and the direction of Snowman's line (figs.5,6 left).

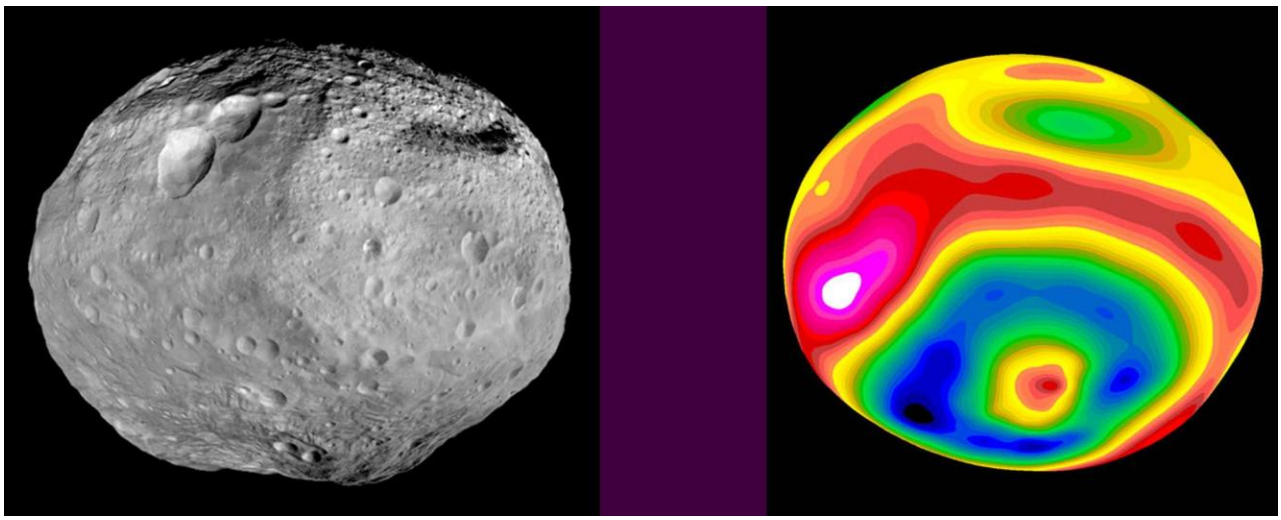

Fig.6. Left: Composite grayscale image of Vesta taken by Dawn spacecraft. Large triple Snowman crater is clearly seen in northern hemisphere. Right: Elevation diagram viewed from the south-east, showing Rheasilvia basin at the Southern pole and Feralia Planitia near the equator (Hubble Space Telescope images).
(https://en.wikipedia.org/wiki/4_Vesta#/media/File:Vesta_full_mosaic.jpg)
(https://en.wikipedia.org/wiki/File:Vesta-Elevation.jpg)

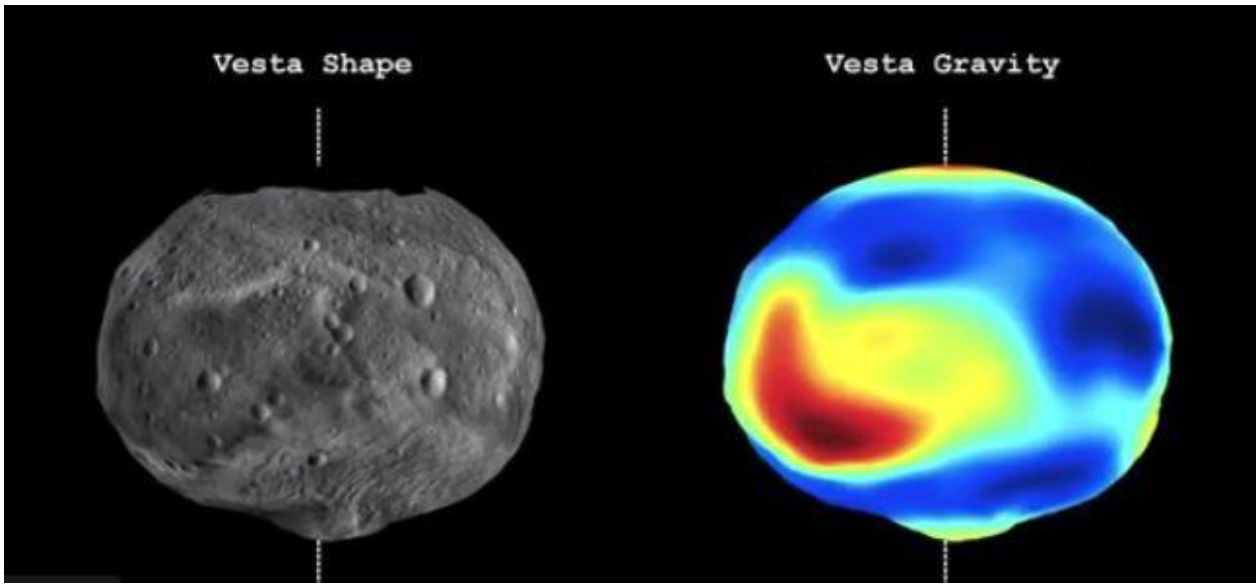

Fig.7. A shot from video: Asteroid Vesta: Topography and Gravity Map - Dawn Mission NASA. (CoconutScienceLab).
(https://www.youtube.com/watch?v=stCm1Ov1Ij8)

The largest vestan crater Rheasilvia is about 500km wide, 19km deep. It obliterates half of Veneneia, other 400km wide basin (see their punctuated borders in fig.9). Rheasilvia's central massive is strangely higher than the crater rims, which broadly resemble hexagon. The basin is oddly located exactly at the southern pole. Central peak is unusual for large craters of the Moon or Mercury where large basins have central depressions. Extensive ejecta deposits and low melt volume in Rheasilvia basin [22] proves its formation in apparently solid state process.

Rheasilvia basin appeared to form because of explosive peeling off southern layers while overall plastic expansion. The disruption is to happen near stress concentrating surfaces including fractures and borders of crustal layers. This scheme is consistent with the similarity of central massive and scarp zigzag relief features near terminator (fig.8, right), with their craterlike streak morphology, and with spiral relief lines in the southern hemisphere. The spirals continue across the borders of the southern basins. Whether they are clockwise or counterclockwise is not clear. The possible explanation is that they reflect differences in southern material's structure. It formed because of Vesta's rotation at the start and were later revealed by surface disruptions.

According to [23] curved ridges at the intersection of Rheasilvia and Veneneia may have been influenced by the Rheasilvia basin relaxation process. Authors of [22] think that unusual spiral fracture pattern is likely related to faulting during uplift and convergence of the basin floor which is consistent with our rationale. The zigzag by-half division of the southern central massive may reflect the development of the vestan global fracture similar to asteroid Steins. The plausible reason of existence of two large basins is that the process of the southern peeling was interspersed by somewhat changes in pole orientation of Vesta. The size disparity of the basins holds a key to their ages.

Fig.8. Left: Processed image of Vesta taken by Dawn on July 24, 2011. The photo in natural colors was acquired from a distance about 5200km. Arrows mark circles of troughs (the equatorial ones are black). Right: Dawn's image of the southern region obtained on July 9, 2011 from 41,000km distance. White curved line to the left shows similar geometry of zigzag relief feature in the center of the polar peak and of scarp line near the terminator. The latter has the morphology usual for crater slopes.
(https://en.wikipedia.org/wiki/File:Vesta in natural color.jpg)
(https://commons.wikimedia.org/wiki/File:Dawn-image-070911.jpg)

There are different opinions on the ages of the southern basins Rheasilvia and Veneneia. One is that they are about 3.570 and 3.770Ga [24], another is 1 and 2 Ga [20,25], respectively. If they are the results of outer impacts it looks strange that the largest craters on Vesta are so young. Contrary, in the frames of our rationale the young formation ages are natural for their evolution stages.

The youngest Rheasilvia age is also consistent with the much lower abundance of Hydrogen and OH-containing materials within the basin compared to the rest of the surface [18]. Besides, younger age is in agreement with the estimates of Vesta asteroid family ages based on dynamical and collisional constraints, supporting the notion that the family was mainly formed during Rheasilvia event [20,22].

There are large-scale families of trough fractures oriented equatorially (fig.8 left, black arrows) and 30° to the north (fig.8 left, white arrows) on Vesta. The poles of the global troughs agree within error with the basin center of Rheasilvia and Veneneia [14]. That geometry suggests their origins to be tied to the origins of the southern basins. Troughs connected to Veneneia (fig.8 left, white arrows) has shallower walls and rounder margins with infilling on the trough floor. They are older.

The authors of [26] evaluated the morphology of the troughs on Vesta and found that the length, width, depth and shape of these features suggest that they are fault-bounded graben. Those impact related graben are thought of as formed because of differentiation of Vesta's interior. It is said in [26] that "it is not unlikely that the strain rate due to giant impact on Vesta would be large enough to result in the instantaneous release of strain in its ductile interior, with concurrent large-scale brittle strain on the surface of the asteroid".

On smaller asteroids fractures or grooves are usually formed. They are revealed on Phobos, asteroids Eros, Ida, ice satellites, etc. Our approach implies the same reason and close genetic relation of graben, troughs, grooves, fractures. They result from stress concentrations and cracking. We will further thoroughly discuss their geometry on example of Phobos' grooves (section 4.5).

The insights into basin and crater formation mechanisms may be given by the results of gamma ray and neutron detections (fig.9). Dawn spacecraft found that vestan regolith contains significant amounts of hydrogen. Zonally averaged neutron counting is systematically higher in the southern hemisphere [18]. The largest hydrogen concentrations correspond to older low-albedo equatorial regions. The youngest Rheasilvia basin has the lowest concentrations. Contrary, Veneneia basin is average in hydrogen contents. Thus hydrogen concentrations provide relative age of vestan regolith.

Craters were found to be the places of local hydrogen minima, for instance, young equatorial crater Marcia with high albedo (fig.9). Solar wind is not enough to explain high hydrogen content. That is why it is explained by outer influx supply of carbonaceous chondrites and gradual accumulation with time. Hydrogen is suggested to be subsequently removed or buried by crater forming outer impacts. Rheasilvia is also depleted of OH materials which are proposed originated gradually during a long term process [19]. Opposite, we think Vesta's hydrogen is endogenous as on the Earth. Hydrogen, helium, methane, etc are known for their ability to extensively seep through the Earth's crust from insides. Besides, the southern hemisphere of Vesta is to have more radioactive materials due to its explosive formations.

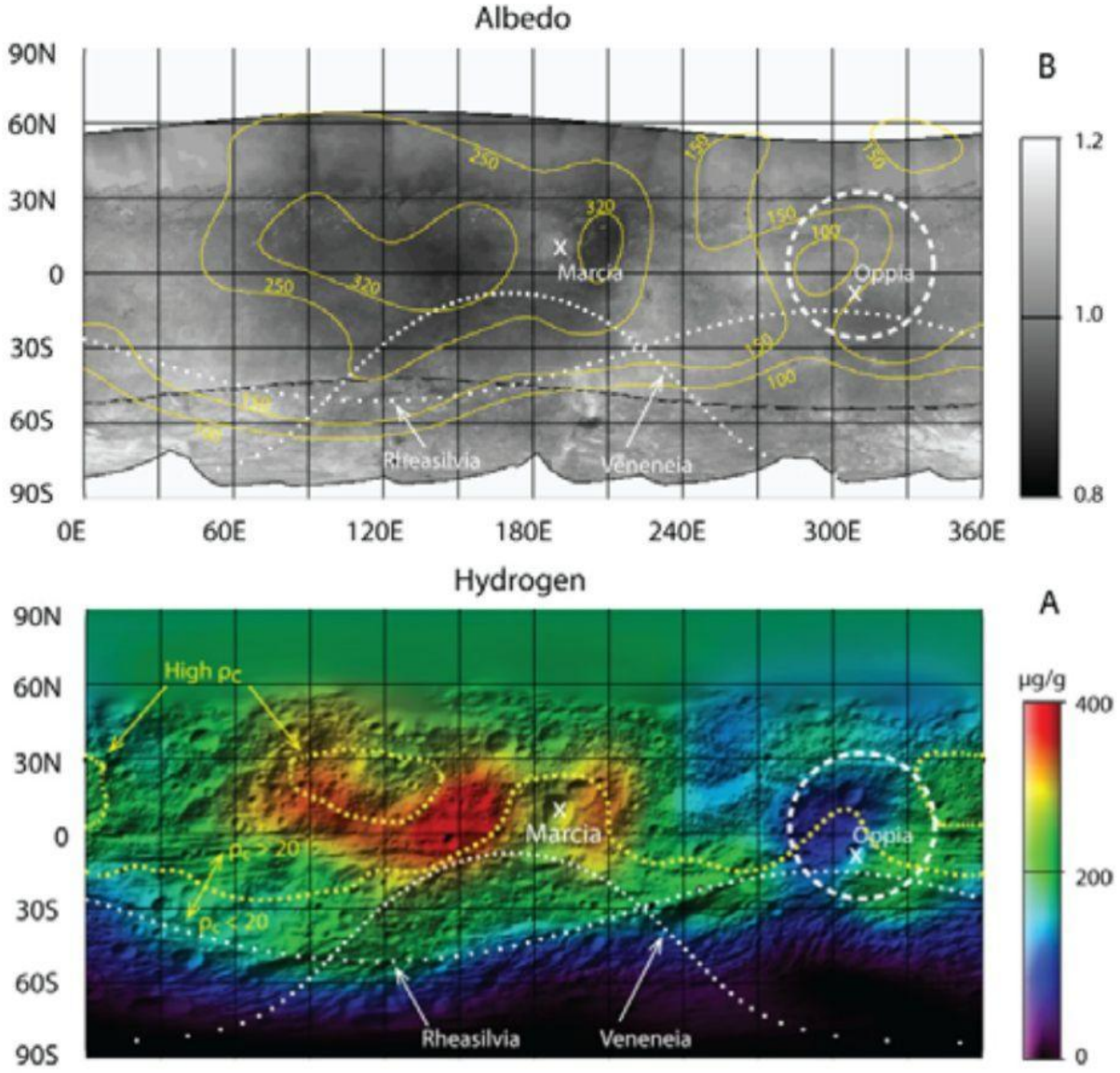

Fig.9. Views taken from Fig.5 of [18] show an albedo map (up) and a map of hydrogen distribution superimposed on shaded relief (down). Yellow contours of hydrogen contents (in μg/g) are superimposed on the map of albedo. The dashed white line outlines a circular depression, containing crater Oppia. Approximate contours of smoothed crater density (ρC in craters per 104 km2), superimposed in yellow on the hydrogen map indicate relative age of the surface.

If one supposes that hydrogen plays crucial role in crustal modifications and crater formations he qualitatively explains the above measurements of hydrogen and hydrogen related substances. Endogenous hydrogen appear to spend while crater formations. It is interesting to see how Vesta's four-fold symmetry repeats in the map of hydrogen contents (fig.9). Therefore the latter is connected to global stress fields. Notice that hydrogen concentration reveals local symmetry of crustal stresses in fig.9, e.g. rhomb-like geometry inside Oppia crater.

4 Formation and evolution of the Martian satellites

4.1 Spectra of the moons

The main problem of all theories of Phobos' and Deimos' origin is the determination of their composition. According to common opinion, spectral data play a key role in that case. Contrary, in the frames of ejective approach surface spectra, as a rule, are not distinctive characteristics of small bodies' compositions due to their explosive high temperature births as well as continuous evolutionary afterbirth modifications of constituent materials [5]. Nonetheless spectra serve important parameters to scrutinize.

Surfaces of the Martian satellites are dark. Near-infrared and visible spectra of the moons are almost featureless. In general the spectra are similar to those of carbon rich chondrites i.e. carbonaceous asteroids. Spectrally the moons belong to (2) Phallas asteroid group [1]. At the same time spectral continuum slope is like that of Martian crust, but albedo is much lower than it is in the darkest regions of Mars. We think the account is continuous formation of carbon containing inclusions with the rate much higher than the one in any region of the red planet.

The spectra confirm that the moons are genetic relatives. Features of Phobos' and Deimos' spectral continuum allow separate two limiting color cases: red and blue units [27]. Difference between the units is tiny, transition between them is continuous. The situation implies no drastic surface compositional or granular diversions. It is also unlikely that redder materials are space weathered bluer materials [1].

Phobos' surface spectra have redder and bluer units, Deimos' spectra has homogeneous redder spectral unit only. Inside Stickney crater either bluer and redder materials are exposed in different locations (see fig.21). That is why Phobos has a bit different spectra of leading and trailing sides [28]. Spectra of Phobos' and Deimos' redder unit are consistent with outer main belt D-class asteroids and Trojan asteroid region. Bluer unit is similar to spectra of P- or T-class asteroids.

Both Martian satellites have darker surfaces than Mars in result of their larger evolution pace. Color difference between Phobos and Deimos also results from the difference in their evolutions. The smaller Deimos evolved with the higher rate. That is why the surface of Deimos is more smooth and relaxed due to plasticity. Phobos has pronounced red and blue spectral units due to the larger scale remains of solid state modifications of its surface by ejective orogenesis.

After tens years of spacecraft explorations majority of researchers are still not quite sure on the compositional analogs of the Martian satellites. We mention only some of research articles to picture the situation. According to [29] composition of the moons remains uncertain. Analyses of red Phobos' and Deimos' spectra and blue Phobos' spectra units made in [30] prove their similarity to those of asteroids, but the authors necessarily recommend specimen taking. The conclusion of [31] is that the moons are captured D-type asteroids. CH and Fe containing phyllosilicates with the spectra like those of primitive bodies of outer solar system regions were implied by the authors to compose surfaces of the satellites. Authors of [1] think that 0.7 micrometer absorption suggests Fe bearing minerals on both moons.

Work [32] proves the presence of phyllosilicates particularly in bluer areas near Stickney while red spectral unit is consistent with tectosilicates, especially feldspars/feldspathoids. The conclusion is made that “no class of chondritic meteorites provide significant agreement with the spectral features observed”. As well “an origin via capture of a trans-neptunian object is not supported by these observations, although it cannot be completely ruled out”. The authors put that, “the most likely scenario is the in-situ formation of Phobos, although a capture of achrondrite-like meteorites is not ruled out”.

According to [33] the moons are dominated by Mars crustal material and may result from giant impact generated accretion. The recent work [34] examines Mars Global Surveyor Thermal Emission Spectrometer mid-infrared data of Phobos and compares them to the laboratory spectra of a suggested D-class asteroids analog C2 meteorite Tagish Lake as well as particulate basalt and phyllosilicate samples, mixed with carbon black to reduce their visible albedos. It was found that “major spectral features in the Phobos spectrum are best matched by a silicate transparency feature similar to that found for finely particulate basalt. Other features in the spectrum are likely best explained by a phyllosilicate component.” Tagish Lake meteorite appears a poor spectral analog to Phobos. The conclusion is that Phobos (and likely Deimos) resulted from Mars as its crust is mostly composed of basaltic rocks.

It was proved in work [35] that (see fig.21) “observations show considerable small-scale heterogeneity, which might be attributable to fresh impacts exposing different materials otherwise largely hidden by a homogenous regolith. The bluer material that is draped over the south-eastern rim of the largest crater on Phobos, Stickney, has been perforated by an impact to reveal redder material and must therefore be relatively thin”.

The ejective rationale leads to similar conclusions. We think that the region south-east to Stickney is covered with the layer of its ejecta which contains bluer substances synthesized during Stickney’s explosive formation. That is the substance of its streaks clearly seen in fig.21. Streaks are possible to form as dykes during ejections or due to downslides [3]. Those formations would not provide severe modifications of initial materials (blue-red spectral differences are not drastic) because of small sizes and gravity of the satellites which escape velocities are diminishing. Small crater formation does not need strong material modification and big explosions. These considerations explain why redder unit substances were thrown out of a bit bluer crater inside large bluer unit area near Stickney (fig.21, black arrow).

Lots of researchers have been trying to decipher Phobos’ and Deimos’ origins on the basis of their spectral resemblance to Mars or to other small bodies. In general, the moons’ spectra appear to be a bit more like the Mars’ ones but have some similarities to those of asteroids. This made us to conclude that commonly considered spectral asteroids-Mars alternative is not correct. The situation is a trap of equating correlation with causation. In Discussion section 5.4 we propose a hypothesis that allow unify spectral results in a broader context of asteroid groups’ and belts’ origins.

4.2 Physical characteristics of the moons

Two small Martian satellites are order of magnitude larger than near-Earth asteroids, several times bigger than main belt asteroid Steins, and order of magnitude smaller than asteroid Vesta (see section 3). The elongated bodies of the moons resemble potato-like asteroids. Dimensions of Phobos and Deimos along main axes of inertia are 26.1x22.8x18.3km and 15.0x12.2x10.4km, average diameters being 22.5km and 12,4km, respectively [1]. The ejective approach accounts for these axes size interrelations in ejected cones and pyramids [5]. The densities of Phobos (1.88g/cc) and Deimos (1.47g/cc) are comparable with the densities of near-Earth asteroids. The near surface densities determined by radar measurements with tens percents accuracy are 1.6 g/cc and 1.1g/cc, respectively [1]. The moons are believed to be layered bodies with inner voids [36].

Phobos is inside Martian synchronous orbit (s.m.a.=9380km), Deimos is beyond it (s.m.a.=23460km). Both orbits are stable, equatorial, nearly circular paths. Phobos' and Deimos' longer X axes are directed towards their parent bodies as is the case for most small bodies in the solar system. It is said in [1, p.13] that "when Phobos' and Deimos' orbits are integrated backward in time, inevitably the moons must once have been in close proximity, raising the possibility that they both formed near a synchronous orbit (37), or even are fragments of a single captured object [38,39)." According to [40] Phobos earlier was near the synchronous orbit of Mars. Deimos was closer to Mars, but not far from its contemporary orbit.

It is obvious that the orbital dynamical data of the Martian satellites are broadly consistent with the ejective model. The other indirect evidences are following. It was found for Koronis asteroid family [41] that the velocities of ejected family members are inversely proportional to their sizes. The functional dependence was explained in [4]. It appears to hold for all ejections by larger parental bodies given certain explosive conditions are fulfilled. Suppose the trend of velocity-on-size dependence to exist in Mars' case. Then larger Phobos was to begin its circular orbital movement closer to Mars than smaller Deimos.

The densities of Mars' crust (2.7-3.7g/cc) [15,16] are higher than those of the moons, but not more than twice. Provided the moons' masses stayed original, the density difference means initial/final size disparities along X,Y,Z to be about several tens percents. The ratios of recent X,Y,Z sizes of the satellites is approx. ½ with the accuracy 10-20%. The ratio hints that the sizes were primarily determined by the ejective instability of the sequential (main and doubled) spatial harmonics in excited crustal layers. If so the Deimos' smaller density and higher velocity are natural due to naturally lower densities of upper crustal layers (see also Discussion section). The ratio appears to suggest similar ages of both satellites.

It is common notion that the Martian moons have shapes completely different from each other (see figs.11,16). Quite opposite, the comparisons of asteroids discussed in section 3 and the Martian moons allow propose that both satellites were initially conical bodies and were thrown by explosive ejection out of Mars' crust into their orbits. Further we confirm the hypothesis and demonstrate how Phobos' and Deimos' shapes stemmed from initial geometries to contemporary ones because of plastic expansions.

4.3 Morphology of Deimos

Deimos's map and views from different sides are shown in figs.10,11.

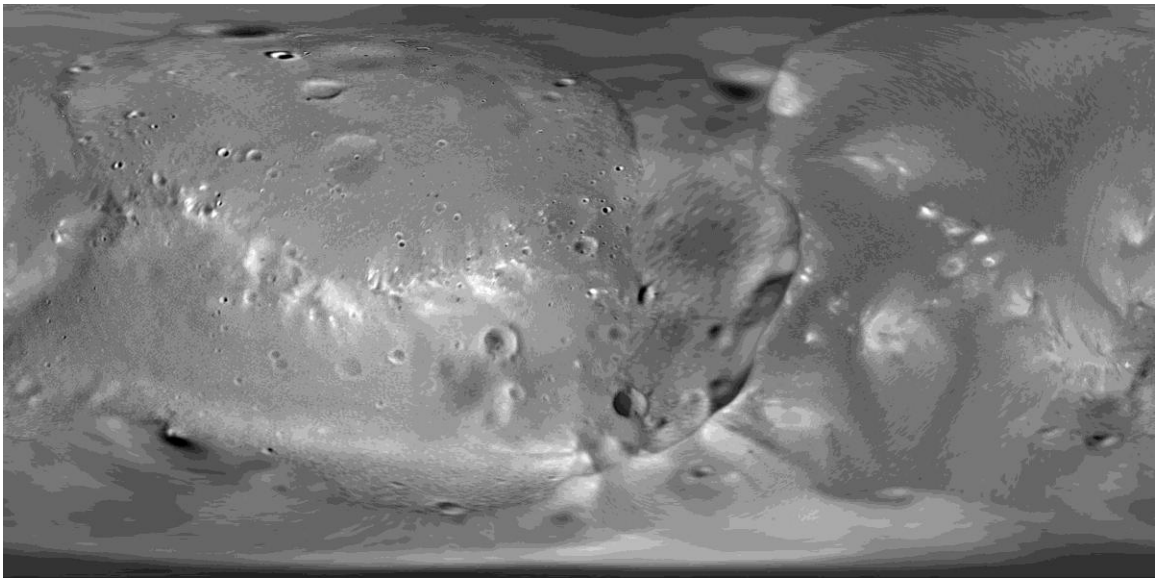

Fig10. Cylindrical map of Deimos created by Philip Stooke with the assistance of Chris Jonkind and Megan Arntz, Control is based on a shape model and mosaic by Peter Thomas and colleagues at Cornell University. (http://solarviews.com/cap/mars/deimoscyl4.htm)

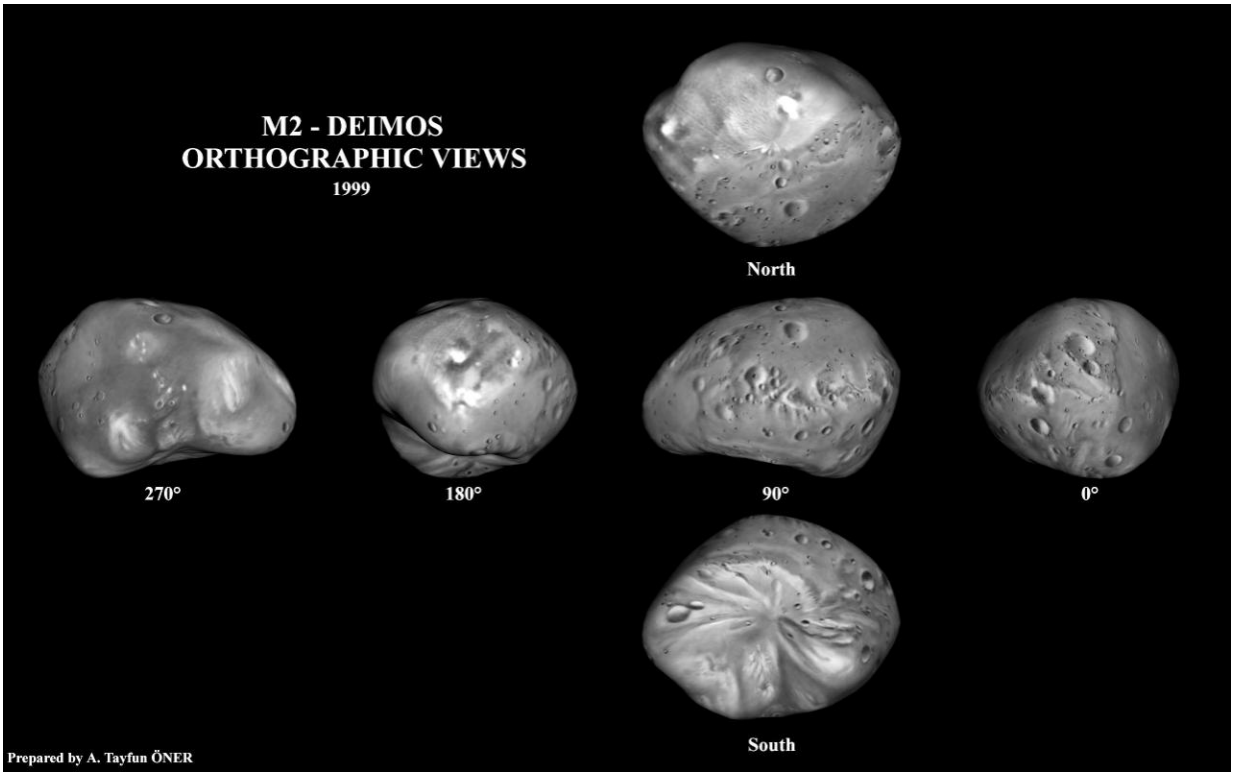

Fig.11. The Deimos' picture (by A.Tayfun Oner) shows six different orientations. The images were rendered by using .P.C. Thomas model and a combination of the USGS map and Deimos' photomosaic. 0° - Sub-Mars hemisphere, 90° - Leading hemisphere, 180° - Anti-Mars hemisphere, 270° – Trailing hemisphere. (http://solarviews.com/cap/mars/deimos6.htm)

Fig.10 gives so to say flowing appearance of Deimos and proves the plastic nature of its evolution. Deimos looks smooth and more liquid-like then asteroid Steins (cf. fig.1). Contrary to Phobos Deimos is blanketed with thick regolith layer. The surface is covered with craters many of which have been partially buried or subdued by regolith. Plastic evolution of the satellite is also confirmed by Deimos' spectra which are even more homogenous than those of Phobos' [30].

Deimos still saves the impression of its initial bulginess. All side views of the satellite show that larger craters are concentrated in the equatorial belt. Equatorial craters resulted from regularly located dykes. The biggest Deimos crater is also equatorial (fig.11, Anti-Mars hemisphere view). The crater is an analog of Phobos' Stickney (see later) and even have similar inner relief features lined at 45° to Deimos' Z axis. Fewer of small Deimos' craters are located near the centers of its geometric facets. The reason is plausible stress concentrations near the borders of large Deimos' constituent blocks.

Side view in fig.12 also proves initial cone-like shape. Cone summit appeared to separate into two unequal parts. The upper one in fig.12 hints on initial truncation of the cone. Also shown are crater lines that are revelations of the layered Martian crustal structure. For example the crater line shown by long black arrow is approximately parallel to the equator which plane was determined by the base of the ejected cone body. The crater line is supposed to form along one of the boundaries of parental crustal layers. In this perspective it is as well parallel to the straight terminator part marked by short black arrow (fig.12, right).

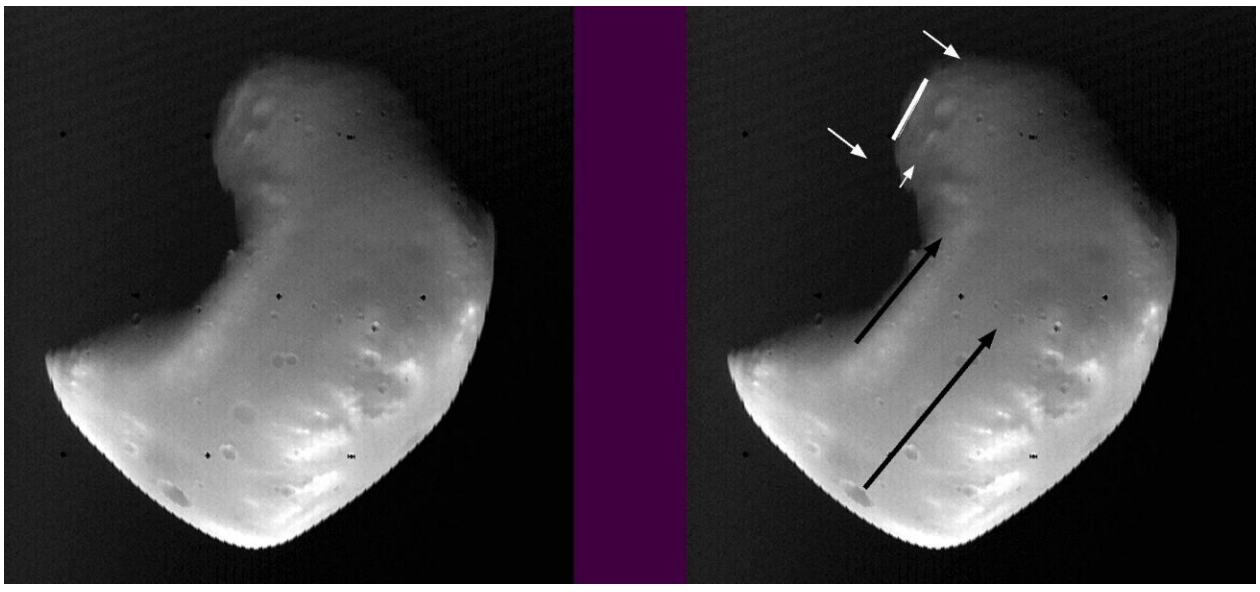

Fig.12.Viking (1977) image of the Martian satellite Deimos taken from 1400 km. The moon is about 14 km from top to bottom in this image. Two longer white arrows approx. restrict the size of possible truncation area. White line is close to hypothetic truncation plane and also marks lined craters. Short white arrow directs another line of craters which is also parallel to the truncation plane. Longer black arrow gives a crater line direction, shorter black arrow marks terminator. Both are approx. parallel to the equator. Color inversion is recommended to see details.
(https://en.wikipedia.org/wiki/File:Deimos-viking1.jpg)

The absence of grooves on Deimos is typically explained by the fact that its orbit is farther than Roche limit. Besides the lack of slow tidal disruption due to tensile stress of Mars there is another reason for Deimos to have no proved groove families en masse as on Phobos. It is plasticity of its surface layers. But Deimos seems to have a couple of grooves in its southern hemisphere (fig.13, left, arrows). Those two groove-like fractures cut the southern hemisphere approx. by half. They are perpendicular to the direction of Deimos' maximal expansion (X axis), i.e. to the orbital radius. The mechanism of their formation appears to be the same as on Phobos (see later).

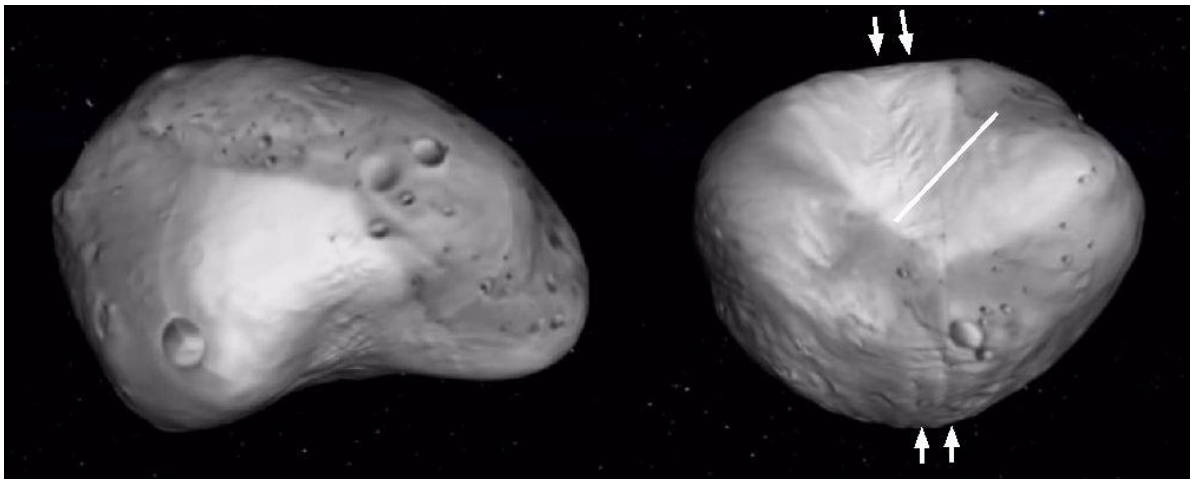

Fig.13. Two shots of Deimos from three-dimensional rotation animation of Phobos and Deimos. Left one is side view, right one is southern view. Directions of two parallel fractures are pricked by arrows. White line shows approximate mirror line of symmetry of local relief.area (Lunas de Marte: Fobos y Deimos visión total 360º. (Copyright: CamenGat. Astronomia creative).
(https://www.youtube.com/watch?v=Mz7Lx3Z-y_I)

Deimos' southern pole is the largest recognized crater (~10km) among solar system small bodies. According to [42] the polar depression is so relatively large that there has been obvious reluctance to classify it as a distinct crater. We think the depression is the result of Deimos' summit rupture and subsequent expansion. This is evidenced e.g. by bright ca. triangle area of contrasted albedo seen in fig.13 (left). One can also find that there are some areas coincident to each other there. The possible symmetry line which approximately mirrors one of them is shown in fig.13. It appears to be at about 45º to the fractures. The opening evolution is not simple elongation. The relief details imply additional rotation which is also proved by smaller line relief details between the two fractures (upper part of fig.13 views) and some others. The details at 45º to the fractures seems to be the result of primary shears.

The expansion of the initial cone apex is also confirmed in fig.14. Spiral relief features which are remnants of cone plastic rotation at the ejective start are clearly seen there. Their curvatures prove that initial rotation was clockwise. Later the apex separated alike, say, untied rope filaments. Complex nature of Deimos' evolutionary elongation is clear. Expansion is obviously different for two global parts of Deimos divided by the global fracture line which comes close to some large craters (figs.14,15). Upper part in fig. 14 shows clear rotation remnants, lower part appeared to rupture perpendicular to the global fracture i.e to the direction of elongation.

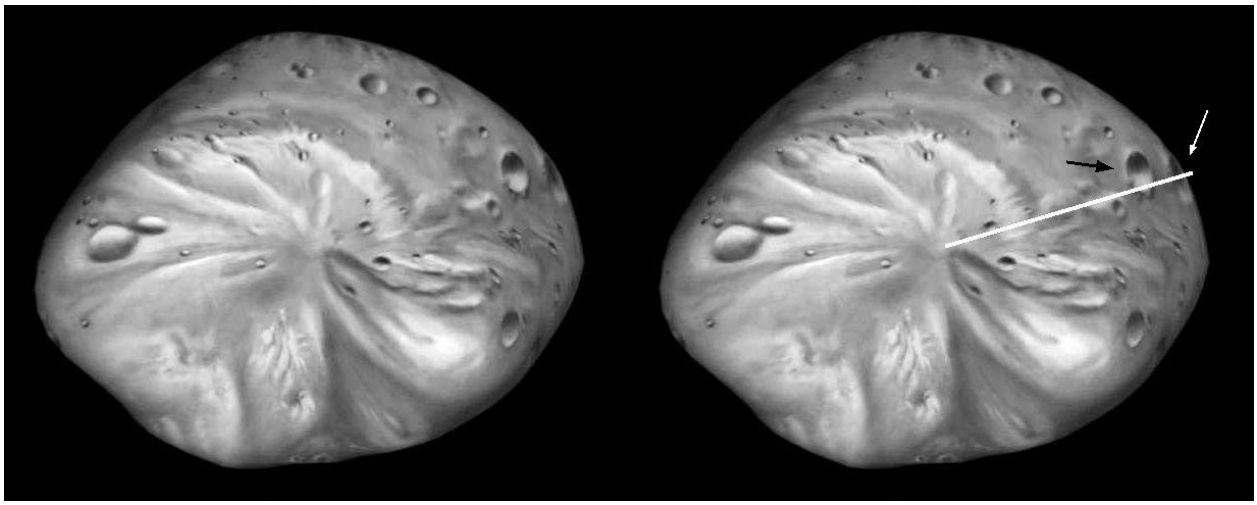

Fig.14. Deimos' southern polar view from fig.11. White line approx. shows possible location of global fracture. Voltaire (white arrow) and Swift (black arrow) craters are located close to the fracture line.

Fig.15. Deimos' northern view acquired by NASA's Viking orbiter. Voltaire and Swift craters are shown with white and black arrows, respectively. (https://commons.wikimedia.org/wiki/File:NASA-Deimos-MarsMoon-19951003.jpg)

The problem of Deimos expansion needs three-dimensional modeling and thorough comparison of relief and compositional details. We are unable to fully restore the development but the evolution tendencies are apparent. The most effective way would be comparisons of mineralogical, substance, and isotope contents of Deimos' surface.

The summit separation almost by half along global fracture is quite usual for small celestial bodies. It leads to formation of two parts of comparable sizes and in the final run results in dog-bone or dumbbell geometries. If we envisage such elongation of a cone-like body divided along its height we exactly get the shape of asteroid Eros. Another dramatic example is comet Hartley 2 with its plastic leaky neck which has no craters and is covered with dispersed rock boulders. According to evolutionary approach the boulders were ejected out of craters which were destroyed by plasticity later. Energetic materials' spewing out into space proceeds at both comet ends while the neck is inactive, this way confirming formation of new substances in the processes of cracking.

4.4 Morphology of Phobos

Morphology analysis of Phobos follows the same logic as that of Deimos. Phobos looks somewhat rounder than Deimos due to more homogenous expansion in all three dimensions. The conclusion is supported by smaller relative deviations of its axial sizes from average values compared to Deimos. Fig. 16 shows that Phobos is also elongated in the orbital radius direction but relatively less than Deimos. Potato shape of Phobos' is usually approximated by an ellipsoid. Phobos' polar views in the first approximation averagely consist of two semicircle parts (of leading and trailing hemispheres) with markedly different radii. In the second approximation the views are hexagonal. The symmetry reflects geometrical interplay of constituent eigenmodes.

Equatorial belt of Phobos is relief emphasized. Largest depressions and elevations are located near it (see also fig.20). Craters of Phobos tend to concentrate along the equatorial belt. The biggest of them crater Stickney (fig.21) is an analog of the biggest Deimos' equatorial crater which is even larger in proportion to the body's size. Stikney is located in between Sub-Mars and leading sides of Phobos, i.e. its center is at approx. 45° to both X and Y axes of the satellite.

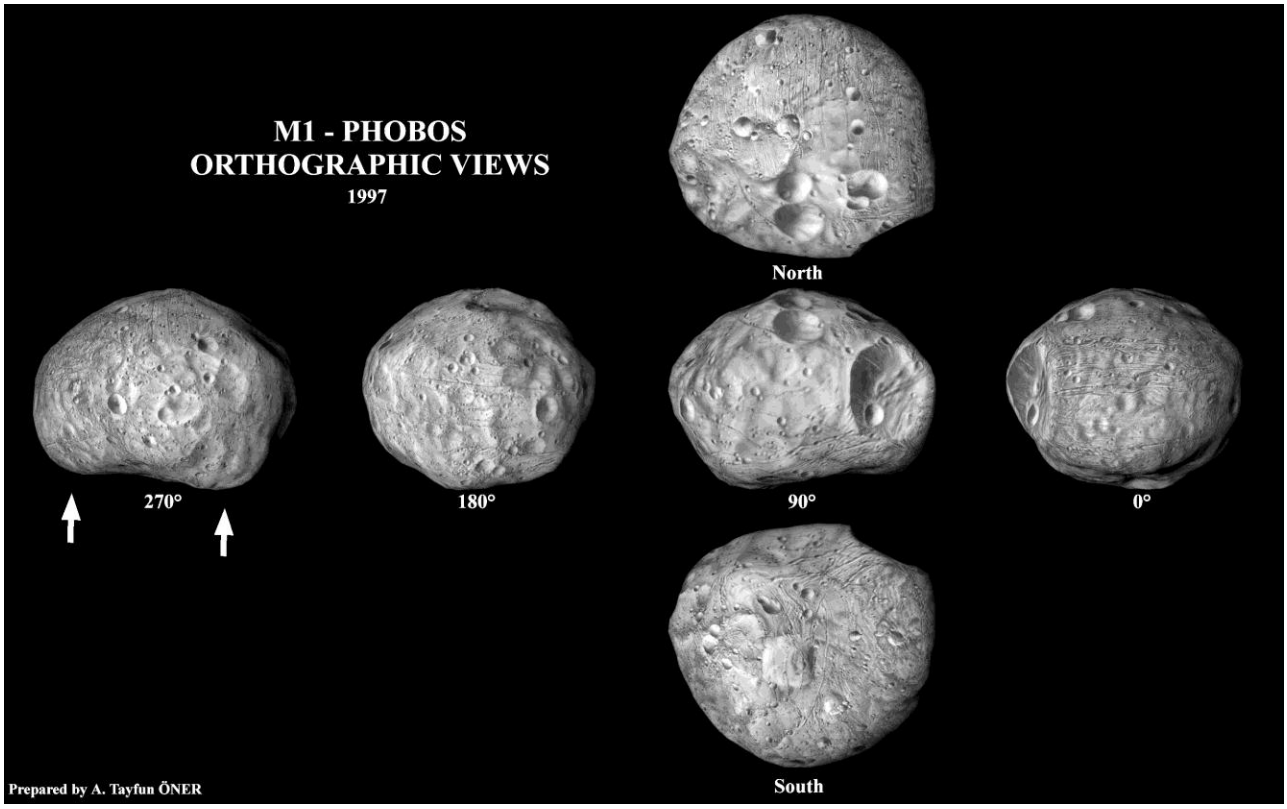

Fig.16. The Phobos' picture produced by A.Tayfun Oner shows six different orientations. The images were rendered by using Peter C. Thomas model and USGS airbush map of the satellite. Middle row: 0° - Sub-Mars hemisphere, 90° - Leading hemisphere, 180° - Anti-Mars hemisphere, 270° – Trailing hemisphere. Phobos' longer axis is directed towards its parent body as is the case for most bodies in the solar system. The remnants of original cone apex separated owing to plastic evolution are pointed by white arrows.
(http://solarviews.com/cap/mars/phobos6.htm)

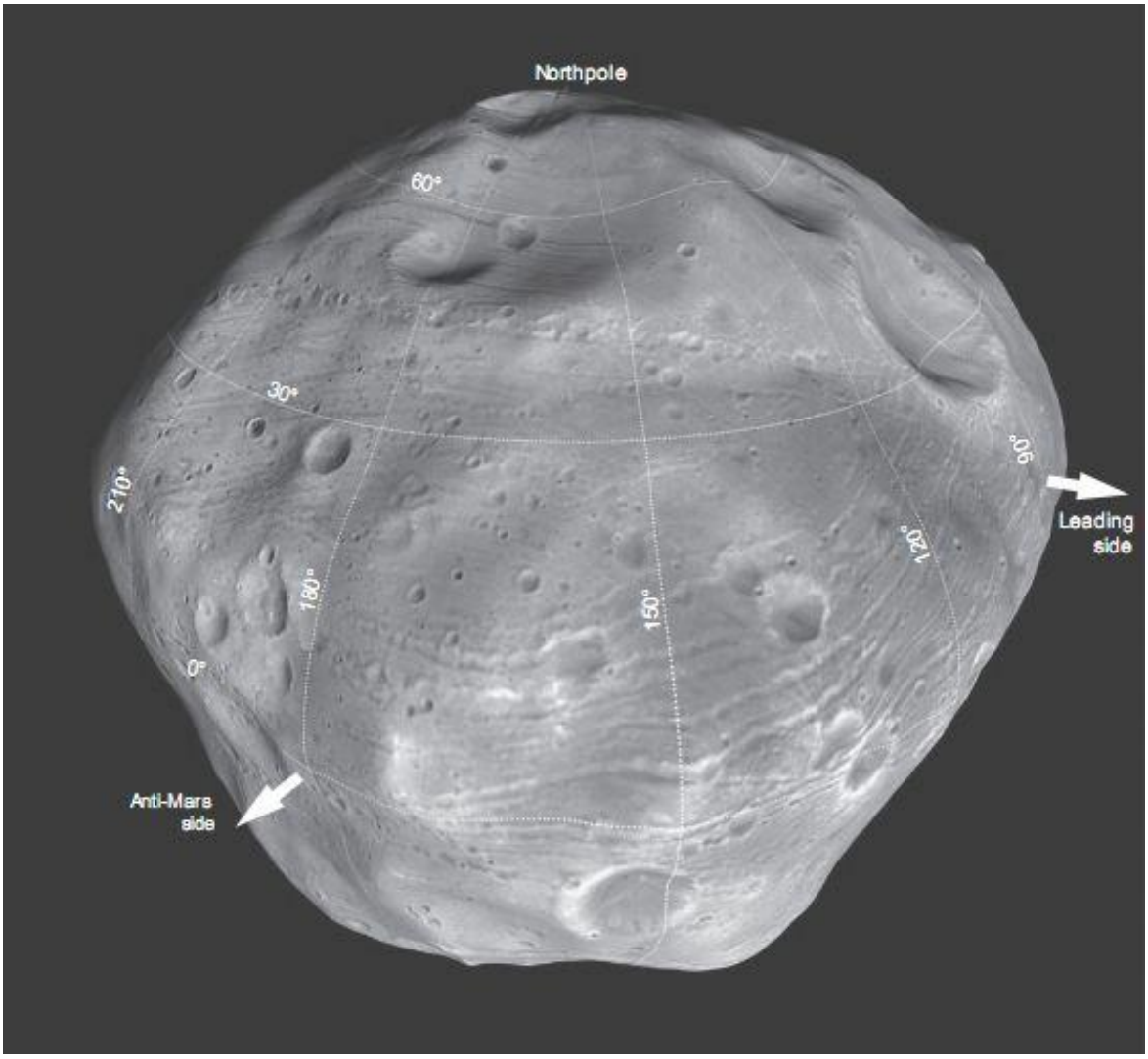

Fig.17. Perspective view of Phobos digital terrain model (fig.6. in [43]) with the draped High Resolution Stereo Camera (Mars Express mission) image mosaic (credit S.Elgner/DLR). Parallel whiter grooves which sometimes degenerate into laced craters are clearly seen in the image. An animation showing Phobos can be viewed at http://europlanet.dlr.de/Phobos/video.

The largest northern craters are lined in the direction perpendicular to that of elongation (see North view in fig.16 and fig.17). It is apparent in fig.17 that big craters are also lined along the middle of Anti-Mars hemisphere. Those crater lines appear to reflect global inner fractures which planes are perpendicular to each other. The fracture quadrant geometry reflects global shape eigenmodes of the satellite.

Evolution expansion of initial southern apex of Phobos is evidenced by its protruding remnants apparent in fig.16 (arrows in Trailing-hemisphere view). Phobos' southern region is more flat in comparison to that of Deimos. The rupture of initial summit, its expansion, and complex history of the polar region are furthermore proved by the similarity if some of its relief features. For example, one of such regions with common for small celestial bodies butterfly or heart-shaped symmetrical geometry is shown in fig.18. Other coincident features are shown in fig.19. Now it is difficult to exactly decipher the regional evolution of sequential expansion. Systematic 3-D modeling and detailed knowledge of local spectra are necessary to thoroughly solve the problem.

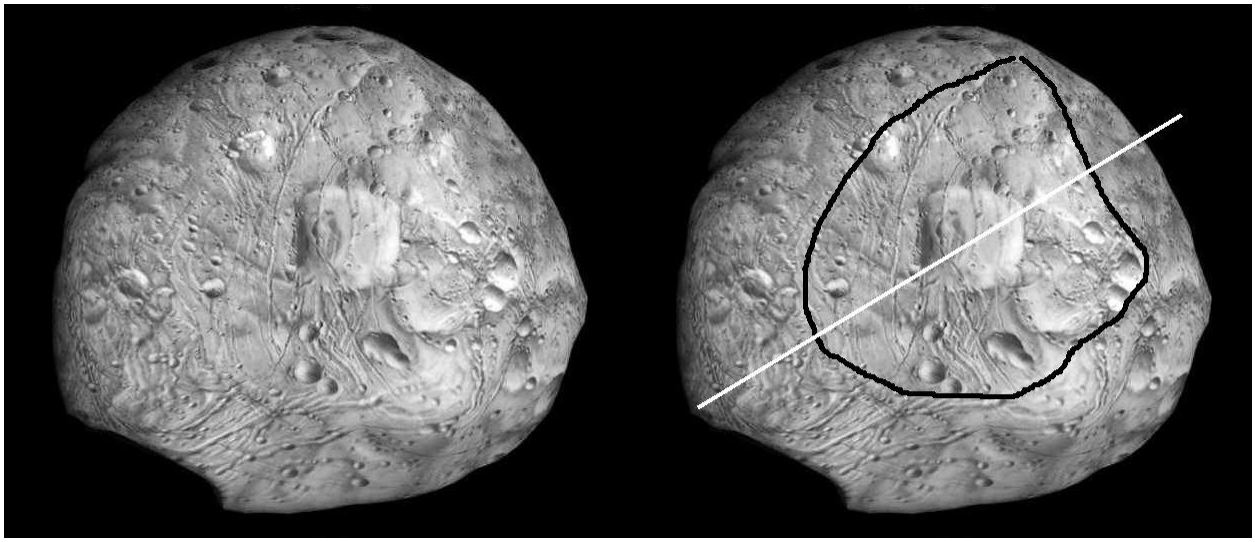

Fig.18. Rotated south polar view from fig.16. Right: butterfly-like relief region is approximately restricted by a black line. White line shows approximate position of mirror line of the butterfly-like region and diagonally crosses rectangular Hall crater.

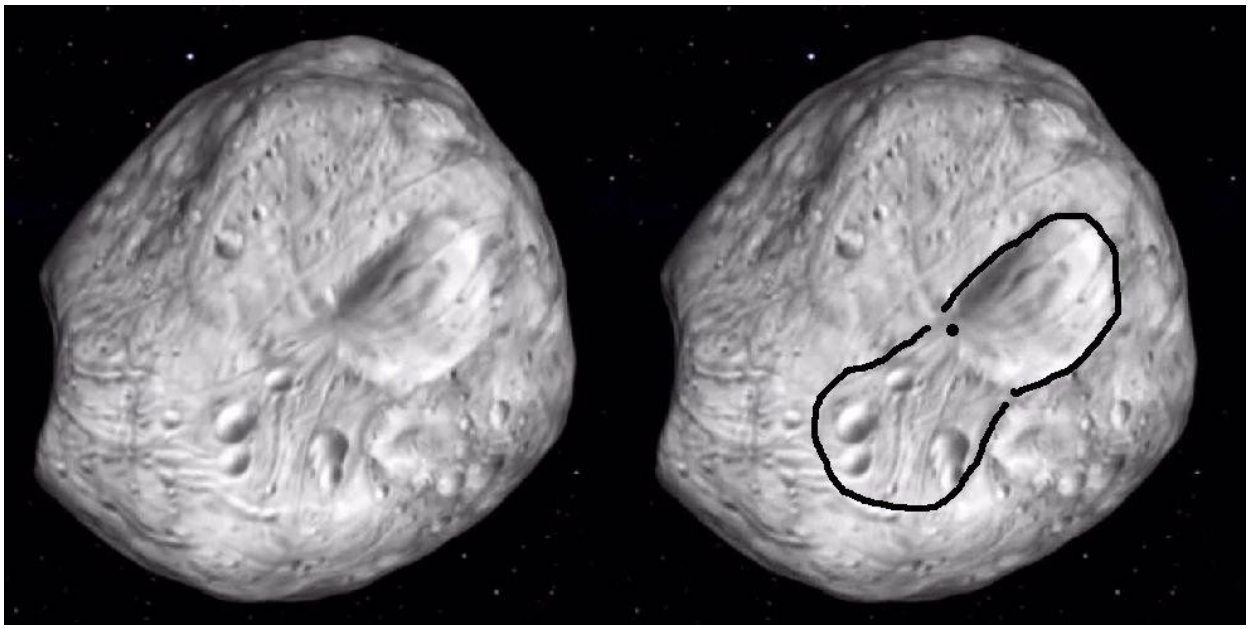

Fig.19. Two shots of Phobos taken from three-dimensional rotation animation of Phobos and Deimos. Right: An elevation with four large craters and coincident to the depression of crater Hall are restricted by black lines. Black point located approx. between symmetrical wings of the two-lobe region ca. marks southern pole of Phobos (Lunas de Marte: Fobos y Deimos visión total 360º.(Copyright: CamenGat. Astronomia creative).
(https://www.youtube.com/watch?v=Mz7Lx3Z-y_I)

All craters of the Martian moons contain brighter materials on their rims which are the evidences of their freshness [3]. Whiter streaks on crater slopes result from dyke formation and explosive materials modifications. They are inherent features of ejective orogenesis [3].

Topography map of Phobos (fig 20) allows put forward hypothesis that equatorial elevations shown in red are remnants of debris ejected from nearby depressions, one of them being Stickney (fig.21) with rim-to-rim north–south dimensions of 9.6km and 9.2km east–west (accuracy 0.5km) [42].

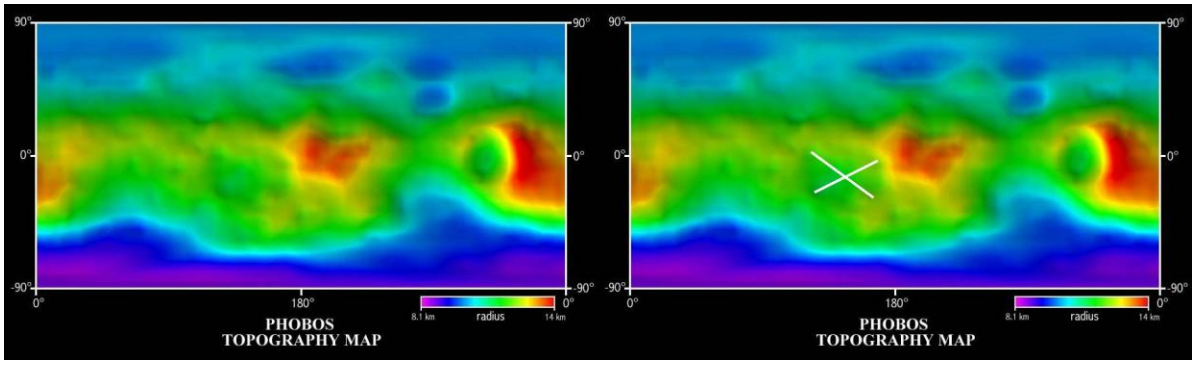

Fig.20. Topographic map of Phobos produced by A.Tayfun Oner and based upon the shape model of Phil Stooke. White cross marks depression geometrically similar to nearby red elevation.
(http://solarviews.com/cap/mars/phobos5.htm)

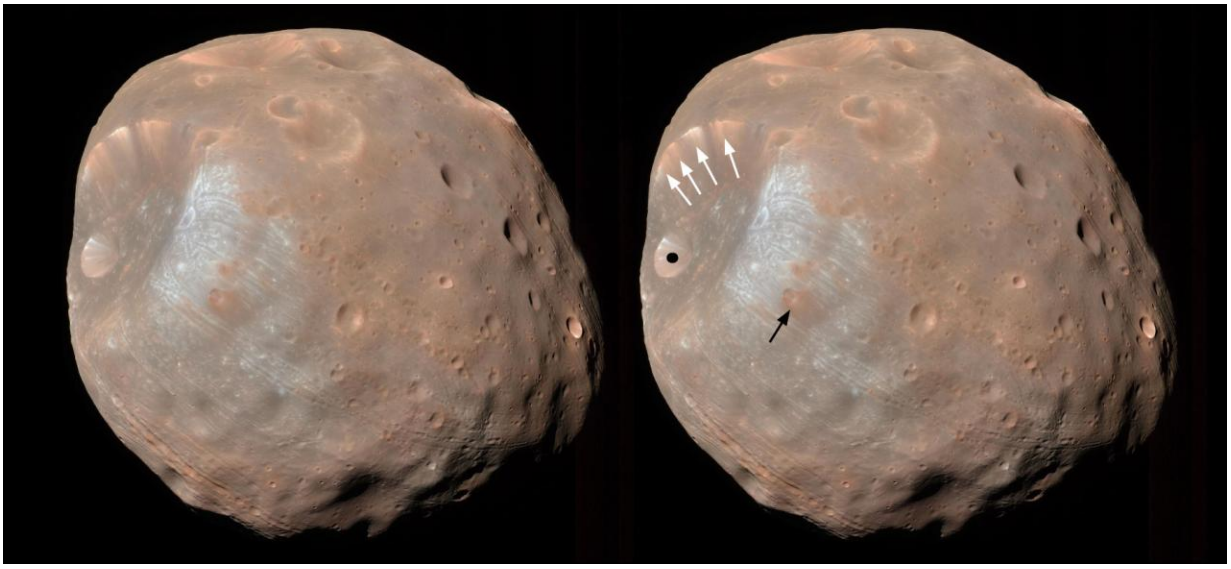

Fig.21.Left: Phobos with Stickney crater imaged by Mars Reconnaissance orbiter on 23 March 2008. Colors combine data from camera's blue-green, red, near-infrared channels. Artificial color data accentuate details of red and blue spectral units. Right: Locations of brighter streaks on Stickney slopes are marked with arrows. Crater Limtoc with similar streaks inside is black dotted. Black arrow points to fresh red unit ejecta of a newly formed crater inside big blue unit area.
(http://photojournal.jpl.nasa.gov/catalog/PIA10368)

In recent calm solar system conditions only small scale events proceed. For instance, sudden ejections of particles from different places of asteroid Bennu's surface were observed by OSIRIS-REx [https://www.nasa.gov/press-release/nasa-mission-reveals-asteroid-has-big-surprises] which proved the predictions of [5]. The Martian moons are also to be geologically active, transient events and dust formation are to regularly happen. Some examples of activity on the moons are discussed in section 5.1.

4.5 Grooves of Phobos

About three hundred grooves feature Phobos [1] but are lacking on Deimos. Grooves are parallel sets of surface depression lines tens meters deep and hundreds meters wide (figs.17,21,22,23). Some grooves are continued by crater chains or consist of regular pits with raised rims which occasionally merge to create a permanent groove. Pits are common for Anti-Mars hemisphere of Phobos. Grooves are usually thought to be of the same fracture origin as on the Moon, asteroid Eros, etc.

Characteristics and features of grooves allow test our rationale on Phobos formation mechanism. In this Section we try to give simple physical explanations for groove properties. Hereafter we are partly making use of excellent description of groove phenomenology given in [44] not separating the article's conclusion on impact mechanism of groove formations.

We suppose that grooves and endogenous craters result from the same physical fracture mechanism of crack opening on different scales which we coined as ejective orogenesis in [3]. Grooves are natural consequences of self-sustainable stresses' development and diffusions of different inhomogeneities. Cracks and disjunctions of different types serve as possible groove precursors due to their ability to concentrate stresses. All larger inhomogeneities are the descendants of their smaller precursors. Grooves are fractures developed and revealed under special stress conditions and may manifest itself or not on the surface and inside a celestial body.

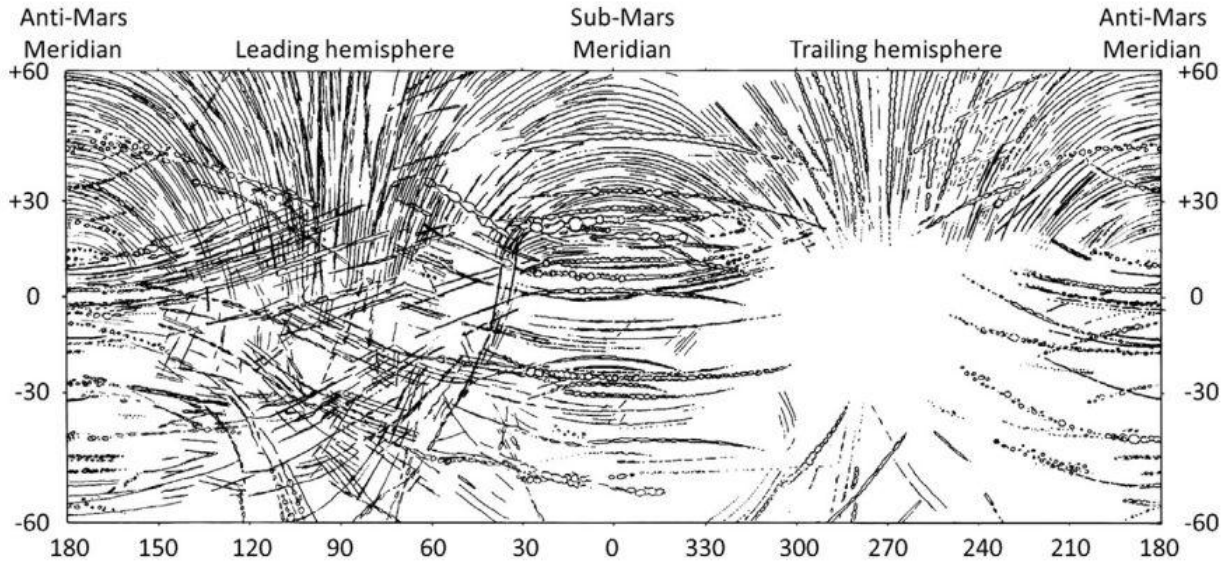

Fig.22. A crop from fig.1 of [44] sketch map of Phobos' grooves (Mercator projection with Phobocentric latitudes), largely based on images from the High Resolution Stereo Camera (HRSC) on board the ESA Mars Express spacecraft.

A groove family is determined as grooves which lie in parallel planes within a few degrees of accuracy. There are even families consisting of few grooves or pit chains. Grooves superpose and intersect each other without offsets. All they have much in common but are supposed to be of different ages. According to [44] there are twelve groove families on Phobos.

The overall groove map is highly symmetrical (fig.22). To our opinion that is due to high symmetries of initial cone-like and recent ellipsoidal Phobos' shapes. The observation that grooves of all different families are parallel only along Sub- and Anti-Mars hemispheres (fig.22) is the consequence of the fact that in Y and Z directions the expansion is lower.

Different families of grooves (see fig.22) cross each other before fading out. Most groovs are close to right or 45° intersections between them and their planes on the surface and inside Phobos. This geometry corresponds to the symmetry of primary shears and tensions. The trailing apex area is the only groove avoidance zone. Here all grooves disappear. There is also zone of overlap antipodal to the zone of avoidance. The avoidance zone looks like undeveloped or degraded zone of overlap.

The existence and geometries of zones seem to be explained by significantly different curvatures of leading and trailing sides of the satellite (see fig.16). The curvatures are related to difference in tensions. The same difference is to produce different regional crater statistics.

Some models consider direct groove formation as resulted from their excavating by mass impacts of small boulders. For instance, the works [45, 46] describe reimpacts of Phobos' orbiting ejecta to form crater chains, termed sesquinary catenae. The article [44] proposes that grooves' crater chains arise from secondary impacts of Mars' ejecta which were generated on its surface by outer impacts.

The work [47] proved strong correlation between the geometry of grooves and surface stress fields produced by Phobos' tidal elongation due to its orbital decay. The theory approximates the satellite as two layer three-dimensional body with weak interior covered by stronger elastic layer. The outcome is that majority of grooves experience tensile stress normal to their strikes. One of the main implications of the analysis is that grooves are "evolutionary progressive". They were brought about after formation of Phobos' main craters because their parallel lines overprint all of them.

Our approach leads to the same conclusion. Large craters appeared at earlier stages of Phobos' evolution. According to the ejective rationale they were the results of excitations of large-scale mechanical modes and resulted in deep crack development. Grooves are disjunctions of smaller scales which evolved later in calmer ambient conditions. Excitations of smaller scale eigenmodes led to the formations of strain fields which were localized closer to Phobos' surface. Surface groove strain accommodates part of large scale stresses. That is why their symmetries are successfully described by the layer model of work [47].

Grooves demonstrate pit behavior which proves the close relations between formation mechanisms of surface lineaments and endogenous concavities. Authors of [44] found that "under the best resolution and illumination, all young grooves can be seen to be crater chains in various states of degradation". Thus grooves are evolving simultaneously with the enlargement of Phobos.

The authors of the tidal model [47] think that Phobos has already started to fail and the grooves are manifestations of the process. The conclusion seems to be questionable because the effect of crack healing is also well known for comets, asteroids, and satellites.

The parallel grooves of the main family dominate most of the northern hemisphere (fig.22). Their planes are perpendicular to the longest axis of the satellite i.e. to the satellite orbital radius because of Phobos' elongation in this direction. The groove plane that passes through the satellite centre also crosses the apex of the leading hemisphere. The plane divides X axis approx. by half which is the result of excitation of second shape eigenmode.

After Phobos' formation as cone-like body its extension led to the division of its summit into two parts. The process was to change inner stress symmetries. One may see in fig.22 that groove crossings are more convenient in the southern region and that they cluster in equatorial zones. Grooves show relative paucity in south and south-east regions of Sub-Mars area, and disappear close to the equator. The reason of the behavior is that tensile stresses were relieved in the southern hemisphere by cone apex rupture. The behavior suggests that it was slow process.

Our basic notion is that Phobos is a coherent layered body ejected by a larger one. That is why after formation it contains remains of all crustal layers (along the polar axis) of his ancestor. After beginning of the evolution the borders between layers serve as stress concentrators which results in the formation of special groove fracture family.

This family J of eleven lines is shown in fig.23**.** Its grooves look direct and almost parallel from their planes. From other points they seem to be curved with "distinctly wavy and disjoint sections due to Phobos' irregular topography" [44]. Comparison of layers' thicknesses with those of the Martian crust is the way to determine places of origin and the ages of Martian satellites. The groove lines also may serve as geodetic lines to measure the displacements of the southern hemisphere during Phobos' evolution.

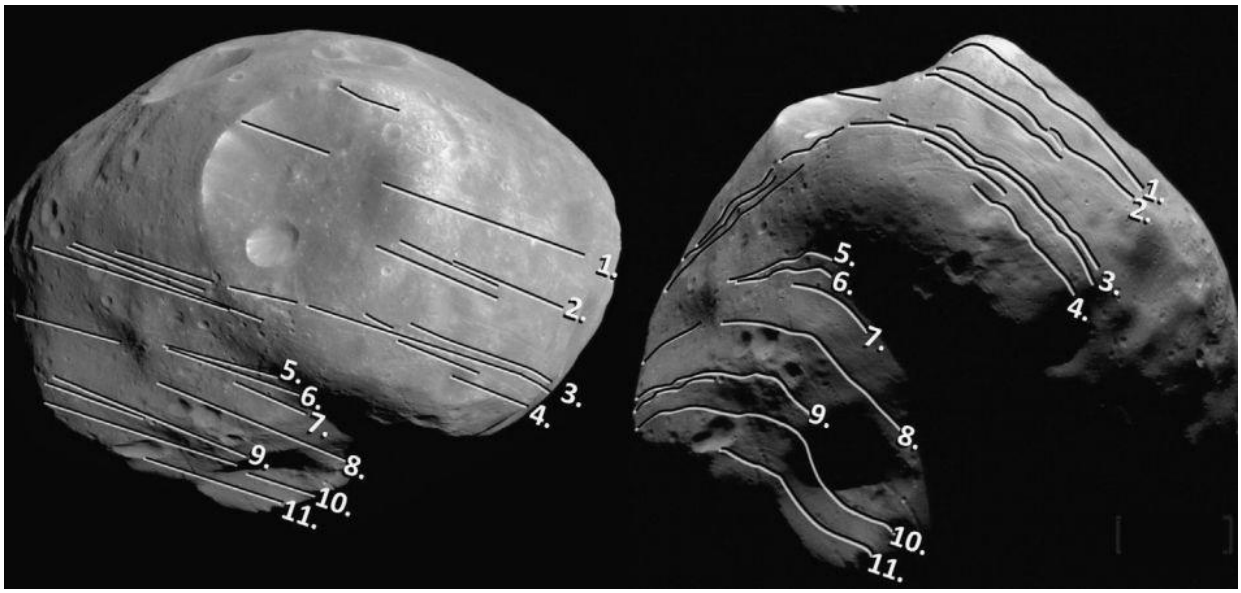

Fig.23 A part of fig.2. from [44] showing the same grooves of family J viewed from close to the planes of the grooves (left) and obliquely to the planes (right). The grooves traced and marked 1 to 11 to aid identification. The large crater at the centre of the left image and at the top of the right one is Stickney.
(Image credit ESA/DLR/FUB, h7479s22 (left) & h7488s22 (right)).

Averagely 150m wide grooves are possible to be about 20 times different in width (25-475m). The largest groove length contrast is 15 times (2-30km) Separate grove craters vary in size approximately 30 times, from 18m which is optical resolution limit to 588m [44]. These facts are not surprising because groove geometry is determined by inner stresses, diverse morphology, and mixed geology of the non-spherical satellite. All groves become thinner closer to their ends. At the same time the crater line density along a groove diminishes. According to our approach the reason is the decay of stress along their fracture lines.

The observation that some craters are a bit elongated in the direction of their crossing grooves also proves the ejective model. It confirms that the direction of tensions that formed both crater and grooves is the same. Sometimes a grove stops abruptly before craters (e.g. fig.4 in ref [44]). The effect is an analog of the stoppage of a crack elongation in, say, a metal case by drilling hole near the crack tip. The reason is that stress intensities and local fractures are determined by tip curvature that is much smaller for a hole.

According to [40] the morphology of grooves is correlated with the distance from Stickney. The deepest and widest grooves are near it. They diminish in size and become smaller on the trailing Phobos' hemisphere roughly antipodal to it. Grooves as fractures opened in regions of weakness may be related to Stickney. It is said in [40], that these openings subsequently developed into grooves either by the drainage of regolith into the fractures, or by the ejection of regolith overlying the fractures, or by a combination of both processes.

Lots of researchers pointed out that prevalent fracture grooves are probably correlated with the location of Stickney crater and originated due to outer impact which formed it [1]. Contemporary observations proved that grooves form no consistent pattern radial to Stickney. At the same time Stickney is the largest crater and its origination may have produced global precursor strains for future fracture formations including surface ones. The consideration may explain the conclusions of [40].

Both Stickney and grooves are determined by stress fields. Stresses produced in Phobos due to the ejection out of Stickney is compatible with contemporary groove symmetry and may have acted in synergy with tensional stresses. Thorough check of the groove-Stickney relations needs three-dimensional numerical modeling of the crater formation.

Our analysis is consistent with that of work [48]. The authors found that "majority of the grooves cannot be explained with the scenarios proposed up to date alone, nor with the impact of the presently visible craters. They concluded that there is "the intriguing possibility that such grooves, if expression of fracture planes, are remnant features of an ancient parent body from which Phobos could have originated. Such scenario has never been considered for Phobos, though this origin was already proposed for the formation of 433 Eros".

5 Discussions

5.1 The origin of Phobos' Monolith and Deimos' alternative

As it was pointed out ejections in contemporary conditions of quiet Solar system evolution proceed on small scales. One such example is weird Phobos Monolith (figs.24, 25.) which special Wikipedia article is devoted to. The Monolith is located near 15°N, 14°W, a few kilometers east of Stickney crater and is likely just a boulder. Common opinion is that it may be a piece of impact bright ejecta 90m high which stands vertically on the surface of Phobos.

.

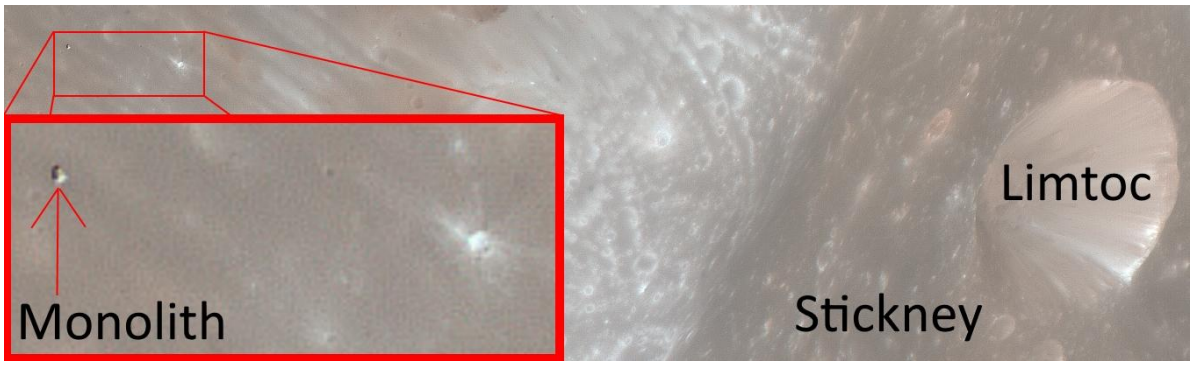

Fig.24 A zoomed-in and labelled part of the public-domain HiRISE image PIA10368 of Phobos, showing the location of the Phobos Monolith, 29 Jan 2016. (https://commons.wikimedia.org/wiki/File:Monolith_Closeup.jpg)

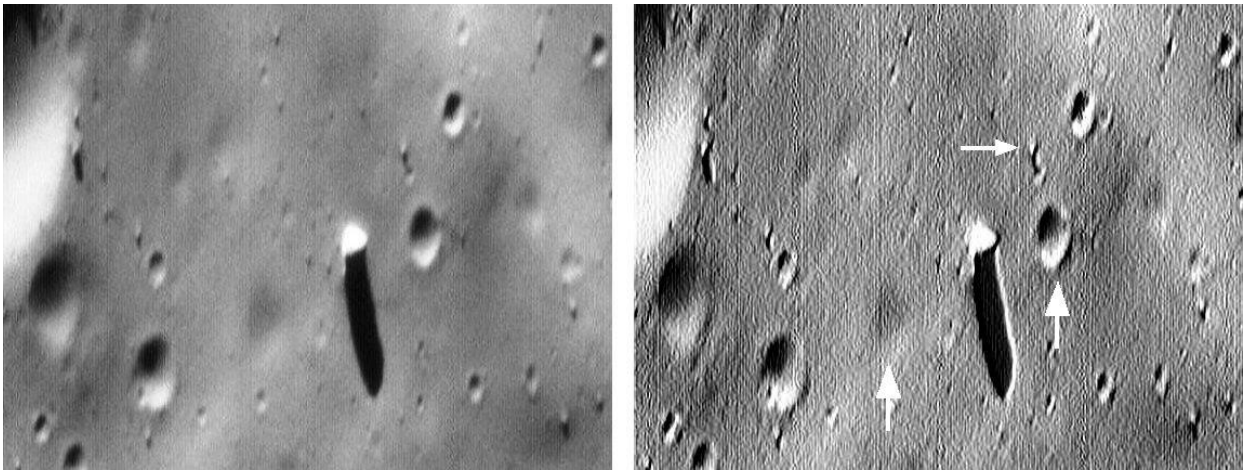

Fig.25. Left: The Phobos Monolith (right of center) as taken by the Mars Global Surveyor (MOC Image 55103) in 1998. The view was cropped from Mars Global Surveyor MOC Image 55103 on 28 July 2009. Right: We applied computational East shadowing (Image J program) to the left image to reveal surface rippling symmetry. Vertical arrows point to possible places of the boulder ejection. Horizontal arrow points to the one of smaller boulders originated the same way. (https://commons.wikimedia.org/wiki/File:Monolith55103h-crop.jpg)

Our proposal is that the Monolith was thrown out of one of the nearest craters. The hypothesis is confirmed by the similar geometry of craters pointed by arrows in figs 24, 25 and by the existence of many analogous small size boulder-crater pairs around.

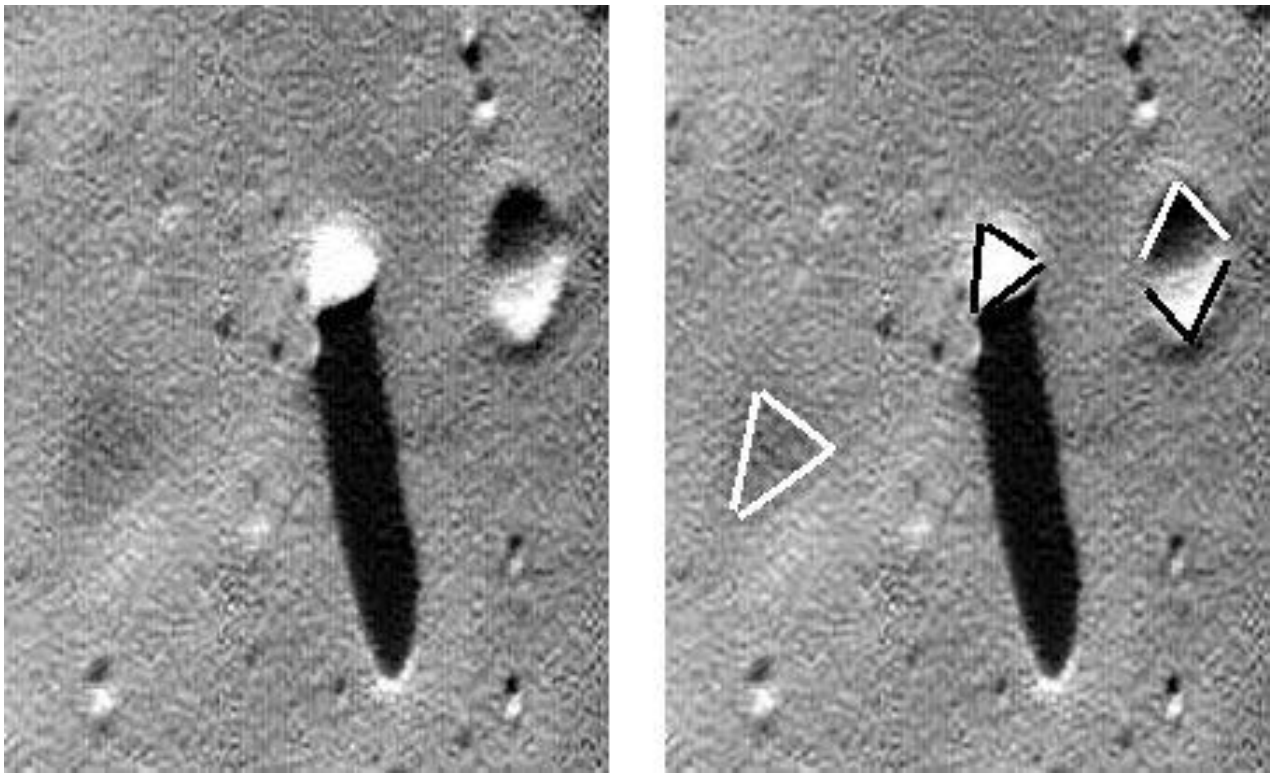

Fig.26. Left: The crop from fig.25). Right: triangles show similar local symmetries.

Programmable shadowing allows find out ripple symmetries of regional Phobos' surface (distorted by inclined illumination and phase angle). Figs. 25, 26 prove that craters are not random. Their locations are determined by local surface corrugations which are connected to regional stress symmetries. They are results of interactions of surface mechanical modes and acquire their symmetries.

The mechanism of ejective orogenesis is the same on global and small size scales therefore shapes of ejected bodies reflect the geometry of stress fields of their birthplaces. The shape of Phobos Monolith and similar boulders prove the possibility of ejections of elongated cylinder-like bodies which are geometrically close to tall truncated cones.

To make the analysis of Deimos' formation alternatives full we are to mention the following hypothesis. Phobos was ejected from Mars' equatorial belt into circular, close to geostationary orbit. Innate to ejective orogenesis singular region (may be even denser than other volume [3,5]) formed at the starting moment and later led to stress concentrations in its vicinity. During subsequent expansion of Phobos Deimos was ejected out of it with simultaneous formation of 9.5km wide Stickney crater.

To asses the scenario's consistency one is to remember that the volume of Deimos is 1000km^3. The volume of an ejected out of Stickney cone with 45° slopes is order of magnitude less. That leads to unreasonable initial densities given Deimos' mass is constant during its evolution. Ejection of a truncated cone with bases' size ratio as in fig.12 and the height of about the Stickney diameter provides afterbirth volume around several hundreds km^3. Therefore the very optimistic assessment gives Initial Deimos' density not less than 4 g/cc (Mars' crust density < 3.7 g/cc). The result is on the verge of reasonability. The evaluations are also consistent with 1-2km inner core of Phobos. We hope that future isotope studies of the moons will verify the Deimos' alternative.

5.2 Ejected boulders of Deimos

There are lots of smaller analogs of Phobos Monolith on Deimos. For instance fig.27 shows craters and nearby boulders in one of the highest resolution images ever taken from an orbiting or flyby spacecraft.

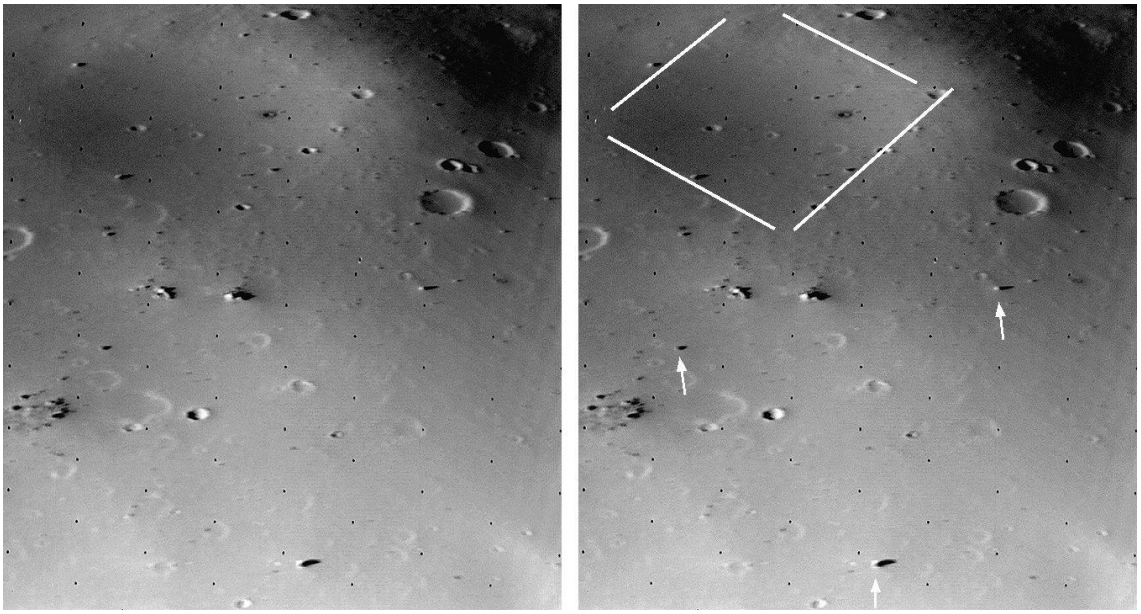

Fig.27. Right: Viking 2 Orbiter image shows the surface of Deimos from 30km. The image covers an area 1.2 km by 1.5 km. North is at 11:30. Features as small as 3m across can be seen. Many craters are covered over by a layer of regolith about 50m thick. Right: Blocks 10-30m across are also visible (white arrows). White lines show local relief surface symmetry also marked by lined craters. (en.wikipedia.org/wiki/Deimos_(moon)#/media/File:Deimos_Surface.png)

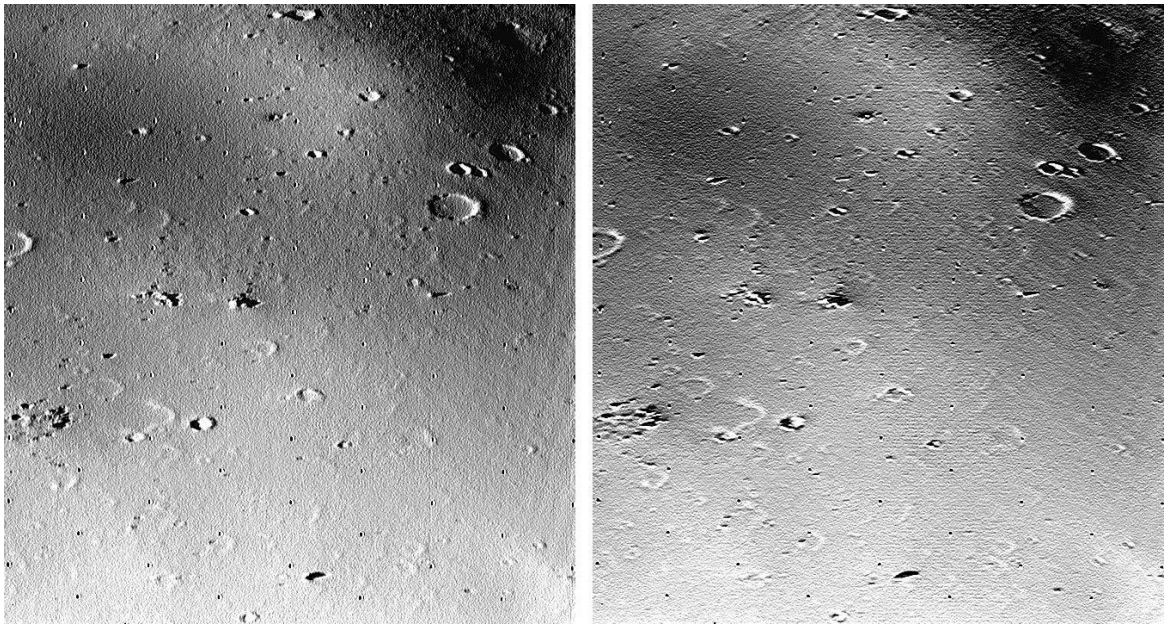

Fig.28. East (left) and South (right) shadowing applied by us to fig.27 reveal surface relief symmetries connected to local stress geometry of upper crustal layers of Deimos..

5.3 Ejective orogenesis on Mars

The surface of the red planet gives abundant examples of the same ejective processes as those discussed for its satellites. Fig.29 shows Mars monolith which is a rectangular object about 5km high. Wikipedia states that it is likely just a boulder and Phobos Monolith is unrelated to it because the latter is located near the bottom of a cliff which it is likely fell down from. Contrary, the figure proves that our conclusions in Sections 5.1 and 5.2 are fully applicable to the situation.

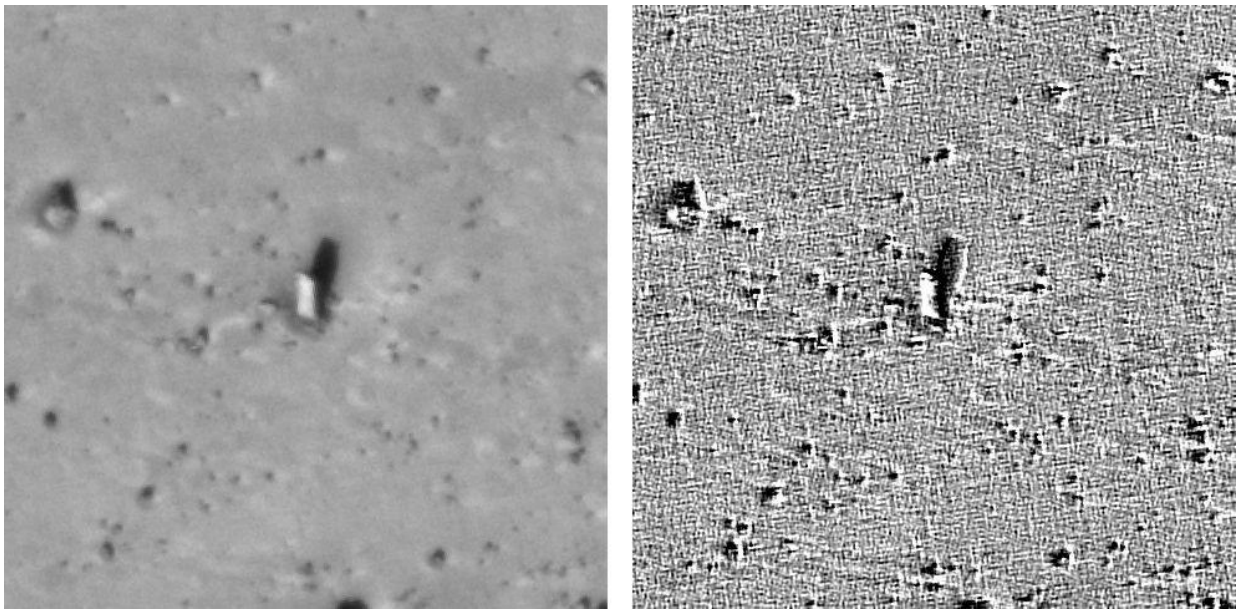

Fig.29. Left: Mars monolith as taken by the Mars Global Surveyor. Right: NE and SE double shadowing was applied to reveal surface symmetry. (https://commons.wikimedia.org/wiki/File:The_Mars_Monolith.jpg)

Many of Martian observations are consistent with the ejective phenomena described in this report. It is widely known that Mars has anomalously large number of craters with nonrandom orientations. The red planet is also famous for pyramid-like boulders and stones dispersed over its surface. For example there exist 20 pyramids in Cydonia region. There happen weird surface splashes, transient events, sudden infill of atmospheric dust, etc on Mars.

Besides, there are strange isotopic anomalies on Mars [49,50]. Especially interesting is Xe129 atmospheric hyper-abundance that was supposed to be stimulated by 14Mev neutrons resulted from hydrogen fusion. K, Th, and U concentrations on Mars surface are much higher compared to those in Mars meteorites, which are believed to be subsurface rocks. Some Mars' meteorites bear the remains of the neutron irradiation. The data hint that thin surface debris layer which is isotope rich was formed by explosion.

Th and K isotopes are abundant in the northern Mare Acidalium (50 W, 55N), less abundant in Utopia Planum (90E, 55N), and have smaller concentration at the globe antipode of the Mare Acidalium spot. Both Mare Acidalium and Utopia Planum contain acid-etched glass [49,50]. Antipode location and smaller concentrations are easily explained by an ejective explosive event because surface waves are to focus in antipodal area.

5.4 Phobos and Deimos in broad contexts

Recent observations demonstrate that proposed ejective formation of the Martian satellites is by no means exclusive or unique. For instance using Hubble Space Telescope astronomers found a small mysterious moon near the largest inner Neptunian moon Proteus [51]. 418km wide Proteus has one of the roughest surfaces known and largest 255km crater Pharos similar to Stickney in location [see e.g. 52]. The tiny moon Hippocamp is 34km in size and three orders of magnitude less in mass. It has the orbit 12000km apart from Proteus. Normally Proteus should have gravitationally swept aside or swallowed the small moon. The articles' conclusion is that Hippocamp is the chipped-off piece of Proteus which resulted from its collision with some comet billions years ago. The ejective explanation of Hippocamp's origination is much simpler and does not need a comet as intermediate stage.

Spectra of redder units of Phobos and Deimos are consistent not only with main belt D-class asteroids but with Trojans [1] which appeared to form similar ejective way. Majority of Mars Trojan asteroids belonging to Eureka family were recently shown to be former parts of Martian crust [53]. Their near-infrared spectra prove that they contain olivine rocks. These are rare among asteroids, but are seen around the largest basins on Mars. Olivine rocks comprise much of Martian mantle and are found in some Martian meteorites. Authors conclude that Mars Trojans are likely to be impact ejecta from Mars.

Volcanic igneous rocks predominate on the red planet. To reconcile orogenesis on Mars and spectral and physical properties of the Martian moons and main belt asteroids we suppose that the belt is the result of explosive ejections from the upper Martian crust. Asteroid densities of the belt do not exceed the crustal densities. Average sum mass of main belt asteroids known with physical accuracy of 10% is 3.3×10^{21} kg. Mars' mass is 6.42×10^{23} kg being about two hundred times more. Therefore several large depressions on the Martian surface are quite enough to provide materials for the main asteroid belt. Different asteroids are possible to be formed out of Martian crust and/or sequentially out of several large bodies ejected by Mars. Common origin of family and non-family main belt asteroids supports the idea. The authors of [54] concluded that main belt asteroids are descendents of several large parent bodies [see also 5].

Work [55] studied complex picture of 93 asteroid binaries. At least four of them appear unpredicted by the working theory of pair formation by rotational fission. Higher primary spins (and kinetic energies) to separate and escape gravities of the primaries are needed. Analyses of 13 pairs with bound and unbound secondaries hints on plausible cascade primary fission formation of them as one of the alternatives. The cascades are sequential fissions of primaries after their regular spin-up. The reason of small (<20km in size) asteroids spin-up is believed to be YORP effect. Larger objects are usually considered to form different way [56].

Spectral features of pair and cluster members are difficult to rationalize [e.g. 57,55]. They are possible to be identical but are usually diverse with different and unpredictable grades of similarity. The situation is alike that for the Martian satellites and other asteroids.

The ejective approach accounts for above observations in a simple manner. Firstly, it incorporates the results of rotational fission mechanism of asteroid pair and cluster formations because ejections of small bodies are special cases of diminutive explosions when minute escape energies are gained by tiny bodies. In those frames the outliers of fission models are naturally clarified by stronger explosive accelerations at the start. Secondly, the approach proves the possible cascade formations of smaller bodies by the larger ones without additional spin-up in result of YORP effect. Thirdly, the approach accounts for all-size origins and logically explains formations of varieties of small celestial bodies.

It is well known that S-type asteroids consist of igneous materials that experienced high temperature and melting. Closer locations of S type asteroids to the Mars' orbit and farther outer belt positions of more carbon containing asteroids is another confirmation of the idea if to follow the logic of evolutionary morphogenesis with continuous enlargements of orbits, density decays, and material modifications. That is the reason of "clear trend of lower bulk densities for primitive objects (C-complex) and higher bulk densities for S-complex asteroids" which was observed in [58].

In general, densities of all dynamical classes of small bodies tend to rise with their sizes and masses. The conclusion is made in [59] for the sample consisting of 17 near-Earth asteroids, 230 Main-Belt and Trojan asteroids, 12 comets, and 28 trans-Neptunian objects. The similar are the results of [60] for Kuiper Belt's Dwarf Planets. Those trends are just what the ejective approach implies because deeper crust has larger density and smaller porosity. Therefore larger parts of mantles and crusts are averagely denser.

Distant Kuiper Belt objects with s.m.a. larger than 230 a.u. are clustered in longitude of perihelion and orbital pole position. Authors of [61] write that "if Planet Nine is not responsible for this clustering, new dynamical processes need to be found in the outer solar system". Explosive ejection of newly formed small bodies provides an alternative explanation of the clustering. Thus the above considerations support the idea of unified formation way of all asteroid belts out of nearest planets' and larger bodies' crusts.

6 Conclusions

We proposed ejective/expansive evolution scenario for the natural Martian moons. According to the model both satellites are former parts of Mars' crust explosively thrown out into their orbits. We confirmed that their newborn cone-like shapes plastically evolved into recent ellipsoid-like ones. The expansions were accompanied by concurrent density decay and simultaneous evolution of their minerals and substances. The gradual plastic morphology changes of the moons during their growths were interspersed by smaller scale explosive ejections with concomitant crater formations. Global ruptures of the southern hemispheres also proceeded.

As clues to the analyses of Phobos and Deimos we used morphologically similar small near-Earth asteroids as well as main belt asteroids Steins and Vesta. Our ejective approach solves the problem of reconciliation of physical and dynamical properties of the moons which has always been the stumbling block of previous schemes. Lots of observational facts are shown to be consistent with the ejective scenario and dozens of the properties are consistently explained.

These includes shaping geometries and moons' divisions into parts by fractures, relations of the ellipsoids' axes and equatorial bulginess, layered inner structures and close-to-equator locations of larger craters, crater line directions and brighter crater streaks, spectral blue/red units and locations of colored ejecta, fracture symmetries on different scales and contemporary geologic activity, etc. Phobos' grooves formation mechanism is described by the same ejective rationale. Their symmetries and locations are made clear by simple physical reasons of fracture mechanics.

The rationale accounts for weird Phobos' Monolith and similar Deimos' and Mars' boulders. Corrugated surfaces of Mars and its moons are shown to be intimately related to the symmetries of all ejected objects. General conclusion is given that the sizes of ejected bodies are nonrandom and connected to the structures of parental warped crusts. Global explosive Martian events are hypothesized to be closely related to the formations of its moons and asteroids.

It was found out that implications of the ejective rationale are consistent with observed characteristics of asteroids. The rationale incorporates known fission mechanism of formation of small (<20km) celestial bodies and naturally accounts for its outliers. The ejective approach explains originations of bodies of all sizes thus providing a unifying scenario. In the frames of it satellites, asteroids, comets belong to the same class of ejected layered celestial bodies.

References

1. Murchie S.L. et al.
   Phobos and Deimos
   In Asteroids IV (P. Michel et al., eds.) U. of Arizona, 1-18, 2015
   doi:10.2458/azu_uapress_9780816532131-ch024.

2. Deutsch A.N. et al.
   Science exploration architecture for Phobos and Deimos: The role of Phobos and Deimos in the future exploration of Mars
   Advances in Space Research 62, 2174–2186, 2018
   doi:10.1016/j.asr.2017.12.017
   available online at www.sciencedirect.com

3. Soumbatov Gur, A.
   Moving mountains and white spots of Ceres.
   Arxiv: 1712.01320

4. Soumbatov-Gur, A.
   Diamonds in the sky. Why ?
   Research Report 2018. HAL-01751079v2
   https://hal.archives-ouvertes.fr/hal-01751079v2/document

5. Soumbatov-Gur, A.
   Predictions for OSIRIS-REx mission at asteroid Bennu
   Research Report 2018. HAL-01883887v2
   https://hal.archives-ouvertes.fr/hal-01883887v2
   doi:10.13140/RG.2.2.32700.90249

6. Accomazzo A. et al.
   The flyby of Rosetta at asteroid Steins – mission and science operations
   Planetary and Space Science 58, 1058–1065, 2010
   doi:10.1016/j.pss.2010.02.004

7. Jorda L. et al.
   Steins: Shape, topography and global physical properties from OSIRIS observations.
   Icarus 221, 1089–1100, 2012
   doi:10.1016/j.icarus.2012.07.035

8. Spjuth S. et al.
   Disk-resolved photometry of Asteroid (2867) Steins
   Icarus 221, 1101–1118, 2012
   doi:10.1016/j.icarus.2012.06.021

9. Ostro S.J. et al.
   Radar Imaging of Binary Near-Earth Asteroid (66391) 1999 KW4
   Science 314, 1276-1280, 2006
   doi:10.1126/science.1133622

10. Scheeres D.J. et al.
Dynamical Configuration of Binary Near-Earth Asteroid (66391) 1999 KW4
Science 314, 1280-1283, 2006
doi:10.1126/science.1133599

11. Brozovic M. et al.
Radar and optical observations and physical modeling of triple near-Earth Asteroid (136617) 1994 CC
Icarus 216, 241–256, 2011
doi:10.1016/j.icarus.2011.09.002

12. Clenet H. et al.
A deep crust-mantle boundary in the asteroid 4 Vesta
Nature 511, 303-306, 2014
doi:10.1038/nature13499

13. Russell C.T. et al.
Dawn at Vesta: Testing the Protoplanetary Paradigm
Science, 336, 684-686, 2012
doi: 10.1126/science.1219381

14. Jaumann R. et al.
Vesta's Shape and Morphology
Science, 336, 687-690, 2012
doi: 10.1126/science.1219122

15. Turcotte D.L. et al.
Is the Martian crust also the Martian elastic lithosphere?
J. Geophys. Res., 107, E11, 5091-6111, 2002
doi:10.1029/2001JE001594

16. Baratoux D. et al.
Petrological constraints on the density of the Martian crust.
J. Geophys. Res. Planets, 119, 1707-1727, 2014
doi:10.1002/2014JE004642.

17. Reddy V. et al.
Color and Albedo Heterogeneity of Vesta from Dawn
Science, 336, 700-704, 2012
doi:10.1126/science.1219088

18. Prettyman T.H. et al.
Elemental mapping by dawn reveals exogenic H in Vesta's regolith
Science 338, 242–246, 2012
doi:10.1126/science.1225354

19. De Sanctis M.C. et al.
Detection of widespread hydrated materials on Vesta by the VIR imaging spectrometer on board of the Dawn mission.
The Astrophysical Journal Letters, 758, L36, 1-5, 2012
doi:10.1088/2041-8205/758/2/L36

20. Marchi S. et al.
The violent collisional history of asteroid 4 Vesta.
Science 336, 690–694, 2012
doi:10.1126/science.1218757

21. De Sanctis M.C. et al.
Across Vesta Spectroscopic Characterization of Mineralogy and Its Diversity
Science, 336, 697-700, 2012
doi:10.1126/science.1219270

22. Schenk P. et al.
The Geologically Recent Giant Impact Basins at Vesta's South Pole
Science 336, 694-697, 2012
doi:10.1126/science.1223272

23. Otto K. et al.
Mass-wasting features and processes in Vesta's south polar basin Rheasilvia
Journal of Geophysical research: Planets, 118, 2279–2294, 2013
doi:10.1002/2013JE004333, 2013

24. Schmedemann N. et al.
The cratering record, chronology and surface ages of (4) Vesta in comparison to smaller asteroids and the ages of HED meteorites
Planetary and Space Science, 103, 104–130, 2014
doi:10.1016/j.pss.2014.04.004

25. O'Brien D. P. et al.
Constraining the cratering chronology of Vesta
Planetary and Space Science 103, 131–142, 2014
doi:10.1016/j.pss.2014.05.013

26. Buczkowski D.L. et al.
Large-scale troughs on Vesta: A signature of planetary tectonics
Geophysical research letters, 39, L18205, 2012
doi:10.1029/2012GL052959

27. Murchie S. et al.
Mars Pathfinder spectral measurements of Phobos and Deimos: comparison with previous data.
J. Geophys. Res. 104, 9069–9079, 1999
doi:10.1029/98JE02248

28. Rivkin A.S. et al.
Near-Infrared spectrophotometry of Phobos and Deimos
Icarus 156, 64–75 (2002)
doi:10.1006/icar.2001.6767
available online at http://www.idealibrary.com

29. Pieters C.M. et al.
Composition of Surface Materials on the Moons of Mars
Planetary and Space Science 102, 144-151, 2014
doi:10.1016/j.pss.2014.02.008

30. Fraeman A.A. et al.
Spectral absorptions on Phobos and Deimos in the visible/near infrared wavelengths and their compositional constraints
Icarus 229, 196–205, 2014
doi:10.1016/j.icarus.2013.11.021

31. Pajola M. et al.
Phobos as D-type captured asteroid, spectral modeling from 0.25 to 4.0 μm
The Astrophysical Journal, 777:127 (6pp), 2013
doi:10.1088/0004-637X/777/2/127

32. Giuranna M. et al.
Compositional interpretation of PFS/MEx and TES/MGS thermal infrared spectra of Phobos.
Planetary and Space Science, 59, 1308–1325, 2011
doi:10.1016/j.pss.2011.01.019

33. Craddock R. A.
Are Phobos and Deimos the result of a giant impact?
Icarus, 211, 1150–1161, 2011
doi:10.1016/j.icarus.2010.10.023

34. Glotch T.D., et al.
MGS-TES spectra suggest a basaltic component in the regolith of Phobos
Journal of Geophysical Research: Planets, 123, 2467–2484, 2018
doi:10.1029/2018JE005647

35. Thomas N. et al.
Spectral heterogeneity on Phobos and Deimos: HiRISE observations and comparisons to Mars Pathfinder results
Planetary and Space Science 59, 1281–1292, 2011
doi:10.1016/j.pss.2010.04.018

36. Busch M.W. et al.
Arecibo radar observations of Phobos and Deimos
Icarus, 186, 581–584, 2007
doi:10.1016/j.icarus.2006.11.003:

37. Rosenblatt P. and Charnoz S.
On the formation of the martian moons from a circum-martian accretion disk
Icarus, 221, 806–815, 2012
doi:10.1016/j.icarus.2012.09.009.

38. Singer S.F.
Origin of the martian satellites Phobos and Deimos.
First International Conference on the Exploration of Phobos and Deimos, Lunar and Planetary Institute, Houston, Abstract #7020, 2007

39. Rosenblatt P.
The origin of the martian moons revisited.
Astron. Astrophys. Rev., 19–44, 2011
doi:10.1007/s00159-011-0044-6

40. Veverka J. and Burns J.A.
The moons of Mars
Ann. Rev. Earth Planet. Sci. 8, 527-558, 1980

41. Carruba V. et al.
Characterizing the original ejection velocity field of the Koronis family.
Icarus 271, 57–66, 2016
doi:10.1016/j.icarus.2016.01.006

Carruba V. et al.
Characterizing the original ejection velocity field of the Koronis family.
Arxiv: 1602.04491

42. Thomas P.C.
Ejecta Emplacement on the Martian Satellites
Icarus, 131, 78–106, 1998
Article No. IS975858

43. Willner K. et al.
Phobos' shape and topography models
Planetary and Space Science 102, 51–59, 2014
doi:10.1016/j.pss.2013.12.006

44. Murray J.B., Heggie D.C.
Character and origin of Phobos' grooves
Planetary and Space Science 2014
doi:10.1016/j.pss.2014.03.001

45. Nayak M., Asphaug E.
Sesquinary catenae on the Martian satellite Phobos from reaccretion of escaping ejecta
Nature Communications 7:12591, 2016
doi:10.1038/NCOMMS12591.

46. Nayak M.
Sesquinary reimpacts dominate surface characteristics on Phobos
Icarus 300, 145–149, 2018
doi:10.1016/j.icarus.2017.08.039

47. Hurford T.A. et al.
Tidal disruption of Phobos as the cause of surface fractures
J. Geophys. Res. Planets, 121, 1054–1065, 2016
doi:10.1002/2015JE004943

48. Simioni E. et al.
Phobos grooves and impact craters: a stereographic analysis
Icarus 2015
doi:10.1016/j.icarus.2015.04.009

49. Brandenburg J.E.
Evidence of a massive thermonuclear explosion on Mars in the past, the Cydonian hypothesis, and Fermi's paradox.
Journal of Cosmology 24(13), 12229-12280, 2014

50. Brandenburg J.E.
Evidence for large, anomalous nuclear explosions on Mars in the past.
46th Lunar and Planetary Science Conference, # 2660, 2015

51. Showalter M.R. et al.
The seventh inner moon of Neptune 2019
Nature, 566 (7744): 350
doi:10.1038/s41586-019-0909-9

52. Croft S.K
Proteus: geology, shape, and catastrophic destruction
Icarus 99, 402-419, 1992

53. Polishook D. et al.
Martian origin for the Mars Trojan asteroids
Nature Astronomy v1, article number 0179, 1-5, 2017
doi:10.1038/s41550-017-0179

54. Dermott S.F. et al.
The common origin of family and non-family asteroids
Nature Astronomy 2, 549-554, 2018
doi:10.1038/s41550-018-0482-4

55. Pravec P. et al.
Asteroid pairs: a complex picture
Arxiv: 1901.05492

56. Margot J-L. et al.
Asteroid systems: Binaries, triples, and pairs.
In Asteroids IV (P. Michel et al., eds.) U. of Arizona, 355–374, 2015
doi:10.2458/azu_uapress_9780816532131-ch019.

Margot J-L. et al.
Asteroid Systems: Binaries, Triples, and Pairs
Arxiv: 1504.00034

57. Pravec P. et al.
Asteroid clusters similar to asteroid pairs
Icarus 304, 110–126, 2018
doi:10.1016/j.icarus.2017.08.008

58. Hanus J. et al.
Volumes and bulk densities of forty asteroids from ADAM shape modeling
Astronomy & Astrophysics 601, A114, 1-41, 2017
doi:10.1051/0004-6361/201629956

59. Carry B.
Density of asteroids
Planetary and Space Science 73, 98–118, 2012
doi:10.1016/j.pss.2012.03.009

Carry B.
Density of asteroids
Arxiv: 1203.4336

60. Barr A.C. and Schwamb M.E.
Interpreting the Densities of the Kuiper Belt's Dwarf Planets
MNRAS 460(2), 1542–1548, 2016
doi:10.1093/mnras/stw1052

Barr A.C. and Schwamb M.E.
Interpreting the Densities of the Kuiper Belt's Dwarf Planets
Arxiv: 1603.06224

61. Brown, M.E. and Batygin K.
Orbital Clustering in the Distant Solar System
The Astronomical Journal, 157:62 (5pp), 2019 Feb.
doi:10.3847/1538-3881/aaf051